

Modern stellar spectroscopy caveats

Sergi Blanco-Cuaresma¹★

¹*Harvard-Smithsonian Center for Astrophysics, 60 Garden Street, Cambridge, MA 02138, USA*

Accepted XXX. Received YYY; in original form ZZZ

ABSTRACT

Multiple codes are available to derive atmospheric parameters and individual chemical abundances from high-resolution spectra of AFGKM stars. Almost every spectroscopist has its own preferences regarding which code and method to use. But intrinsic differences between codes and methods lead to complex systematics that depend on multiple variables such as the selected spectral regions and the radiative transfer code used. I expanded iSpec, the popular open source spectroscopic tool, to support the most known radiative transfer codes and I assessed their similarities and biases when using multiple setups based on the equivalent width method and the synthetic spectral fitting technique (interpolating from a pre-computed grid of spectra or synthesizing with interpolated model atmospheres). This work shows that systematics on atmospheric parameter and abundances between most of the codes can be reduced when using the same method and a careful spectral feature selection is executed, but it may not be possible to ignore the remaining differences depending on what is the scientific case and the required precision. Regarding methods, equivalent width-based and spectrum fitting-analyses exhibit large differences that emerge due to their intrinsic differences, which is relevant given the popularity of these two methods. The results help us identify the key caveats of modern spectroscopy that any scientist should be aware of before trusting its own results or being tempted to combine atmospheric parameters and abundances from the literature.

Key words: stars: fundamental parameters – stars: abundances – stars: atmospheres – techniques: spectroscopic

1 INTRODUCTION

The automation of high-resolution stellar spectra analysis for AFGKM stars has become a necessity in the latest years due to the enormous increase of publicly available observations. Large surveys such as APOGEE (Eisenstein et al. 2011; Majewski et al. 2017) or the Gaia-ESO Public Spectroscopic Survey (GES; Gilmore et al. 2012; Randich et al. 2013), complemented by smaller surveys like OCCASO (Casamiquela et al. 2016, 2017) plus other independent studies and observational proposals, have contributed to this golden period of stellar spectroscopy.

Several research groups have developed different codes to analyse all these data and some have made their work openly available (e.g., SME Valenti & Piskunov 1996, GALA Mucciarelli et al. 2013, FAMA Mucciarelli et al. 2013, StePar Tabernero et al. 2013, iSpec Blanco-Cuaresma et al. 2014b, The Cannon Ness et al. 2015, ZASPE Brahm et al. 2017, FASMA Tsantaki et al. 2018). Except those methods that

use the whole spectrum (or a single continuous spectral region) for their analysis (e.g., MATISSE Recio-Blanco et al. 2006, FERRE Allende Prieto et al. 2006, ULySS Koleva et al. 2009, Starfish Czekala et al. 2015, sick Casey 2016), most of them base the analysis on certain spectral features.

Deriving atmospheric parameters and abundances from stellar spectra can be generally done by following two different strategies: the equivalent width method and the synthetic spectral fitting technique. The equivalent width method first requires to measure equivalent width of a selection of neutral and ionized iron absorption lines. This is generally done by fitting a Gaussian profile, and computing the width of the spectral continuum that has the same area as the absorption line. Then, a radiative transfer code is used to derive individual line abundances for a given set of initial atmospheric parameters. The stellar parameters are found by flattening the abundance trends with respect to reduced equivalent width, lower excitation potential, and ionisation stage. In the case of the synthetic spectral fitting technique, the observed spectrum is compare to theoretical spectra that is synthesized on-the-fly or interpolated from pre-computed grids (in both cases, a radiative transfer code is also neces-

★ E-mail: sblancocuaresma@cfa.harvard.edu

sary) and a minimization algorithm is executed. Frequently, a selection of spectral features is used instead of the full spectrum to reduce computation time and concentrate on the more informative spectral regions. The previously mentioned codes generally follow one of these two strategies.

In addition to the significant diversity of codes available, any of them can be set-up with many different combinations of necessary ingredients such as the grid of model atmospheres (where interpolations are needed to derive the right model for the desired atmospheric parameters), the solar abundances of reference (which can be scaled up or down following the desired metallicity, or certain elements can be enhanced/depleted to follow certain patterns such as the enhancement of alpha elements observed for metal poor stars), the radiative transfer code, the atomic data (e.g., wavelengths, oscillator strengths, line broadening parameters such as the radiative/Stark/van der Waals damping parameters), the selection of spectral features to use (e.g., some regions may carry more information than others or simply some codes and models are better at reproducing these regions), or the continuum normalization procedure. These inhomogeneities have lead to large discrepancies in the atmospheric parameters and abundances present in the literature (Hinkel et al. 2014).

The source of this problem was first explored in Hinkel et al. (2016), where four spectra were analysed using six different codes with subsequent re-analysis with common atmospheric parameters and atomic line lists to determine chemical abundances. The study showed that homogenizing atomic data and atmospheric parameters lead to an improvement on the agreement between abundances derived by each method although the dispersion kept being high for several elements. The authors concluded that it is necessary to further investigate inherent issues between the different spectroscopic techniques.

The same problem was tackled again even more thoughtfully by Jofré et al. (2017), where four abundances were determined for four Gaia Benchmark Stars (Jofré et al. 2014, 2015; Heiter et al. 2015b; Hawkins et al. 2016) using six different methods and one representative line for each of the four elements with fixed atmospheric parameters (i.e., effective temperature, surface gravity and metallicity). The study showed that equivalent width methods are less affected by shifted absorption lines, synthesis methods need to implement mechanisms to detect the shift and perform a correction. The agreement between methods improved when a common normalization was applied (see also a briefly discussion about normalization effects in Sect. 4.1 in Blanco-Cuaresma et al. (2015)) and when the same microturbulence was used, however this parameter is very sensitive to the method used which leads to the impossibility of having a good criteria to define a good common value for all the techniques. The neglect of hyperfine structure (i.e., shifts and splittings in the energy levels of atoms, molecules, and ions, due to interaction between the state of the nucleus and the state of the electron clouds), and different assumptions on the abundances of blending elements contribute to increase discrepancies. Different atmospheric model interpolation methods lead to very small differences, only relevant if very high precision abundances are required. For equivalent width methods, differences arise from the use of different radiative transfer codes. For synthetic methods, different line

masks (i.e., spectral region that includes the target absorption lines) does not seem to lead to any significant difference but differences in broadening parameters does.

These studies have glimpsed the first clues behind the discrepancies currently found in the literature for spectroscopic analysis. However, they are limited to a very low number of spectra and the execution involved several different research groups using their own codes with, sometimes, manual operations. Despite the excellent coordination, it is easier to make mistakes when the analysis is not fully automatic or when a completely homogeneous analysis cannot be guaranteed. Revealing the essential caveats of modern spectroscopy requires fully automatic and reliable tests that analyse homogeneously a higher number of spectra covering a wider range of stars.

In this work, I have extended iSpec¹ (Blanco-Cuaresma et al. 2014b) by: 1) including a large number of radiative transfers codes widely used for spectral synthesis and equivalent width analysis (Blanco-Cuaresma et al. 2017; Blanco-Cuaresma 2017); 2) adding spectra interpolation capabilities which allows the user to use/compare a different spectroscopic approach (i.e., spectra interpolation instead of model atmosphere interpolation). iSpec has become a great tool for spectroscopic analysis but also a very convenient framework to discover and assess the caveats of modern stellar spectroscopy. Using this tool, I designed several fully automatic experiments that compares the impact of using distinct radiative transfer codes, different setups and spectroscopic techniques.

2 DATA

The Gaia FGKM Benchmark Stars (Jofré et al. 2014, 2015; Heiter et al. 2015b; Hawkins et al. 2016) is a set of very well-known stars covering a wide range in effective temperature (3500 - 6600 K), surface gravity (0.50 - 4.60 dex) and metallicity (-2.70 - 0.30 dex). They are especially convenient for spectral analysis assessments since they are accompanied by atmospheric parameters of reference obtained from methods independent of spectroscopy.

For this work, I used the high-resolution spectra provided by the public library² (Blanco-Cuaresma et al. 2014a). The original non-normalized spectra comes from different instruments with different resolution, spectral ranges and signal-to-noise ratios (S/N). Some pre-processing was executed to homogenize the dataset, including merging separate wavelength regions from the same observation, co-adding spectra to increase the S/N, cleaning areas affected by telluric lines (i.e., set fluxes to zero), correcting radial velocities, estimate the S/N and error fluxes (which strongly influences derived parameter errors), selecting the spectral range of 480 to 680 nm (optical range) and degrading the resolution to 47 000, which matches the resolution and range of the UVES set-up used in the Gaia-ESO Survey.

¹ The iSpec version used in this work was released as v2019.03.02

² <http://www.blancocuaresma.com/s/>

3 PIPELINE

3.1 Methods

iSpec can derive atmospheric parameters using the synthetic spectral fitting technique and the equivalent width method. The former compares the observed fluxes (weighted by the flux errors if present) with synthetic spectrum for a selected set of spectral features, then a least-square algorithm minimizes the differences (i.e., computing the χ^2) by varying the atmospheric parameters until convergence is reached. The spectral features can be absorption lines or any other spectral region. For instance, it is common to use the wings of H- α / β and Mg triplet to help break degeneracies given that these regions are highly sensitive to effective temperature and surface gravity, respectively. The synthetic spectra can be computed on-demand by interpolating from a grid of model atmospheres and using a radiative transfer code, or now also by interpolating from a grid of pre-computed spectra with iSpec or another tools (this also opens the possibility of using grids of synthetic spectra for cooler or hotter stars than AFGKM or even grids of observed spectra). In both cases, the input grid is used to construct convex hulls and a linear barycentric interpolation is executed at each necessary triangle. No specific code was written for this, I used widely tested methods present in the Qhull and SciPy packages (Barber et al. 1996; Jones et al. 2001).

In the case of the equivalent width method (which also requires model atmosphere interpolations), the analysis starts with a selection of absorption lines produced by neutral and ionized iron for which their equivalent width is measured. Usually this is done by fitting Gaussian profiles and determining the area of each absorption line. Then the equivalent width can be transformed to abundances by using a radiative transfer code, and the atmospheric parameters will be varied until there is no correlation between abundances and equivalent widths, and excitation equilibrium plus ionization balance is reached (i.e., no correlation with excitation potential and the average iron abundance from neutral and ionized lines is equal). In this case, no other spectral features different from iron absorption lines are used and the analysis is fast given that the amount of information is smaller compared to synthesis methods (i.e., the full line profiles are not considered, only their area).

In this work I am going to compare: 1) the synthetic spectral fitting technique using a grid of atmospheric models; 2) the synthetic spectral fitting technique using a grid of pre-computed synthetic spectra; 3) the equivalent width method.

3.2 Radiative transfer codes

For all the method described in Sect. 3.1, iSpec offers a broad variety of radiative transfer codes (a summary can be found in Table 1). It is worth noting that all these radiative transfer codes assume local thermodynamic equilibrium (LTE), which means that the mean free path of photons is smaller than the scale over which thermodynamic quantities vary, thus the atmospheric state (e.g., temperature) at a given depth is affected by radiation below or above that point. This approximation is not valid for OB stars or extremely metal-poor stars which have optically thin layers where non-local non-thermal influences (i.e., radiation) overcome local

thermalising ones (i.e., collisions). Nevertheless, the approximation is good enough for AFGKM stars depending on the kind of analysis and scientific goals.

Most of the codes use model atmospheres calculated assuming plane-parallel geometry, hence the radiative transfer is solved neglecting the curvature of the atmosphere and only considering one depth variable. This is a valid approximation for most stars but it breaks down when the stellar atmosphere size starts to be relevant compared to the stellar radius (e.g., cold giants and supergiants). Only some codes can consider the curvature when providing model atmosphere that were calculated assuming a spherical geometry.

All the codes were integrated in iSpec in the most homogeneous possible way, this implies that certain default behaviours were overridden. For instance, codes such as SYNTHExtract the abundances from the model atmosphere input file while others, such as MOOG, have default hard-coded values that can be modified if the user issues the right commands. Additionally, certain functions provided by these codes were not used such as resolution degradation, macro-turbulence and rotational effects. To guarantee comparable results, these effects are directly implemented in iSpec and they are homogeneously applied to all synthetic spectra independently of what radiative transfer code generated it. Researchers that make use of these tools outside the iSpec framework should expect differences that were minimized for this work.

3.2.1 SPECTRUM

SPECTRUM version 2.76e³ (Gray & Corbally 1994) is a radiative transfer code written in C (compatible with the gcc compiler) that can synthesize spectra and derive abundances from equivalent widths. However, the later is done by fully synthesizing each absorption line and it is computationally expensive (i.e., significantly slower) compared to MOOG or WIDTH9, which uses the faster direct computational analysis (Gray 2008, chapter 16). I did not use it for the tests based on the equivalent width method but it is an ideal code for the synthetic spectral fitting technique since it is one of the fastest.

3.2.2 Turbospectrum

Turbospectrum version 15.1⁴ (written in Fortran and compatible with the gfortran compiler Alvarez & Plez 1998; Plez 2012) is similar to SPECTRUM in terms of usage and I also excluded it from tests based on the equivalent width method. Contrary to SPECTRUM, which only works with plane-parallel model atmospheres, Turbospectrum can use spherical models (they offer a better approximation for giant stars) where the stellar radius and the depth of each layer has to be provided (as shown in Table A1).

³ <http://www.appstate.edu/~grayro/spectrum/spectrum.html>

⁴ <http://www.pages-perso-bertrand-plez.univ-montp2.fr/>

	SPECTRUM	Turbospectrum	SME	MOOG	WIDTH9/SYNTH
1D plane-parallel model atmosphere geometry	✓	✓	✓	✓	✓
1D spherical model atmosphere geometry		✓	✓		
NLTE					
Grids of NLTE departure coefficient			✓		
Customizable chemical abundances	✓	✓	✓	✓	✓
Customizable isotopes	✓	✓		✓	
Customizable molecular dissociation constants	✓	✓		✓	
Re-computed model atmosphere electron density	✓	✓	✓		✓
Continuum scattering		✓	✓		
Radiative damping parameter due to natural broadening	✓	✓	✓	✓	✓
Stark broadening due to collisions with charged particles	✓		✓		✓
Classical van der Waals damping parameter	✓	✓		✓	✓
Anstee and O'Mara van der Waals broadening theory	✓	✓	✓	✓	✓
Hydrogen broadening	AG	BPO	BPO	BPO	AG
Customizable hydrogen lines parameters		✓	✓	✓	✓
Base line profiles	Voigt	Voigt	Voigt	Voigt	Voigt
Average synthesis time in seconds (480 - 680 nm)	~123	~56	~222	~68	~360

Table 1. Summary of radiative transfer code features. Customizable stands for the possibility to change values without recompiling the program, BPO stands for Barklem-Piskunov-O'Mara (Barklem et al. 2000), and AG stands for Ali-Griem (Ali & Griem 1965, 1966).

3.2.3 SME

SME version 4.23⁵ (Valenti & Piskunov 1996) is the only considered radiative code that is closed source, which makes its debugging and scientific assessment more difficult. It is distributed with IDL scripts that call a pre-compiled binary library which performs the spectral synthesis, iSpec only uses this library. SME only does synthesis and, equivalent to Turbospectrum, it can work with spherical model atmospheres. The code is ready to consider departure coefficients for NLTE effects, although this has not been considered for this work.

3.2.4 MOOG

MOOG version February 2017⁶ (Snedden et al. 2012) is a radiative transfer code written in Fortran (compatible with the gfortran compiler) which can synthesize spectra and derive abundances from equivalent widths efficiently. Unfortunately, MOOG depends on the non-free SM package (formerly SuperMongo) for plotting results. Given that iSpec already has its own free python interface, I developed a SM package mock with the same functions but empty implementation which allow us to compile MOOG without the real non-free SM package. This is the only code that does not recompute electron densities but it keeps them fixed them as provided by the input model atmosphere.

3.2.5 WIDTH9/SYNTH

WIDTH9 version 9 March 1993 and SYNTH version 20 July 2001⁷ (Kurucz 1993; Sbordone et al. 2004) are programs that share the same radiative transfer code but the former is used to transform equivalent widths into abundances, while the latter is the one that computes synthetic spectra. Both are written in Fortran and require the Intel compiler, which is not open source (contrary to gfortran), thus already pre-compiled executables are included in iSpec by default. More details about this code can be found in Cowley & Castelli (2002).

3.3 Model atmosphere

For the grid of model atmosphere grid I used MARCS⁸ (Gustafsson et al. 2008), which was computed with solar abundances from Grevesse et al. (2007). Notice that iSpec also support ATLAS/Kurucz and many other solar abundances, but MARCS includes models computed with plane-parallel and spherical geometries. The latter allow for spherical radiative transfer (although only with codes that support it, as explained in Sect. 3.2) and it ensures a more realistic temperature structure of the model atmospheres as the spherically symmetric radiative transfer scheme takes into account the geometric dilution of flux. The spherical radiative transfer is generally not important for line formation,

⁵ <http://www.stsci.edu/valenti/sme.html>

⁶ <http://www.as.utexas.edu/chris/moog.html>

⁷ <http://atmos.obspm.fr/>

⁸ <http://marcs.astro.uu.se/>

but very important for the model atmosphere structures (Heiter & Eriksson 2006). iSpec uses the model atmosphere grid to construct convex hulls where linear barycentric interpolations at each necessary triangle can be executed to generate the required model with the necessary atmospheric parameters (always within the grid ranges). Regarding the radiative transfer codes, not all of them require the same model atmosphere input values, the differences are shown in Table A1.

3.4 Atomic data

The atomic data used in this work corresponds to the line list version 5 from the Gaia-ESO Survey line list (Heiter et al. 2015a). The line list format is automatically transformed by iSpec to fit the requirements from every radiative transfer code. Also, some lines are not used for certain codes if they are not compatible or necessary. For instance, SPECTRUM has several hard-coded strong absorption lines (which should not be included in the atomic line list or it would generate twice strong lines): Hydrogen-line series (Lyman, Balmer, Paschen, Brackett, Pfund and Humphreys), thirty-one Helium I lines, eleven Iron II lines, one Magnesium I line and two Magnesium I lines, one Calcium I line and two Calcium II lines, one Scandium II line, and one Strontium II line. Turbospectrum and MOOG include also their own data for Hydrogen and Helium lines. All these already included lines will not be taken from the GES line list when using these codes.

In terms of isotopes, SPECTRUM documentation indicates that it supports 311 atomic isotopes plus 40 molecular isotopes and their relative abundance can be fine-tuned using an input file. The rest of the codes do not seem to offer this possibility (they have hard-coded values) and are less well documented, this makes homogenization and comparison difficult. Apart from filtering out isotopes not supported by SPECTRUM, no other atomic data selection has been performed based on isotopes.

Regarding molecules, not all the codes support the same molecules and SPECTRUM is again the best documented code, while Turbospectrum seems to be the code that more molecules support. Furthermore, every code includes their own dissociation energies for molecules and only SPECTRUM (via the input solar abundance), MOOG (via the input line list) and Turbospectrum (via specific molecule input files) allow the user to override them without modifying the source code. In any case, the public version of the GES line list does not include molecules (only relevant for the coolest Benchmark Stars).

In all the cases, I discarded atomic lines for 2nd or higher ionized atoms (e.g., Fe III), lines with lower state excitation potential higher than 15 eV and auto-ionising transitions for metals (corresponding to only 20 and 17 lines, respectively) to reduce computation time since their contribution is small for FGKM stars and they are also not supported by all the codes.

Regardless of starting with a common atomic line list, there are differences that arise due to the intrinsic functioning of each code. Moreover, not all of them use the same input values as shown in Table A2. Sometimes the differences are just a matter of units or format, but in other cases there are values that are not required at all by some codes.

3.5 Line selection

No matter if the analysis method is based on equivalent width or synthetic spectral fitting technique, the spectral ranges used in the study are going to have a relevant impact on the final derived atmospheric parameters. Given the nature of the methods used in this work, most spectral ranges are going to correspond to absorption lines since they carry key information related to the atmospheric parameters of the star.

It is common to find studies in the literature where authors use a line selection done by other authors, but this approach implies risks. A line might be good when using a specific spectroscopic pipeline with a concrete set-up (e.g. normalization process, atmospheric models, radiative transfer codes, atomic data) and observed spectra with a particular resolution, but dramatically bad when any of these components change. For instance, a line selection done with high-resolution spectra might not be convenient for lower resolutions since lines can be blended: equivalent width methods will over-estimate the abundance and synthetic spectral fitting techniques might provide in-accurate results if the near-by lines have bad atomic data.

A strategy that minimizes some of these difficulties is to follow a purely line-by-line differential approach. For instance, this could be done by calibrating the absorption lines' $\log(gf)$ value to better reproduce each line profile in a reference star with very well-known atmospheric parameters (typically, the Sun) and then use this calibrated atomic data to derive atmospheric parameters. In the case of equivalent widths, a different but equivalent approach is to measuring the abundance of all the lines in a reference star, subtracting the result for all the lines measured in the target star, and using these differential abundances (instead of absolute abundances) to reach ionization balance and excitation equilibrium.

Nevertheless, given the goal of this study, I preferred to avoid the calibration of $\log(gf)$ values and use the same atomic data for all the different radiative transfer codes. This avoids introducing another degree of freedom that might make the comparison more difficult, although it makes the line selection process particularly important.

I used the NARVAL solar spectrum with the highest signal-to-noise ratio in the Gaia Benchmark Stars library for the line selection process described in the following subsections. The spectrum was convolved to a resolution of 47 000, corrected from its radial velocity and normalized following the same procedure as any other spectra in this study.

3.5.1 Matching absorption lines to atomic data

The first required step in the line selection process is to identify which lines from the GES atomic line list are the main contributors to the observed absorption lines in the solar spectrum. For this, first I only considered lines from the GES line list which have a theoretical depth greater than 0.01 and a reduced equivalent width⁹ greater than -7 for solar atmospheric parameters. Then, I used iSpec to fit

⁹ $\log_{10}\left(\frac{EW}{\lambda}\right)$ where EW is the equivalent width and λ is the wavelength position

Gaussian profiles for all the lines in this subset and I discarded those which fit has failed or has a depth greater than 1 or lower than 0.01. There may be more than one close-by atomic line (closer than 0.001 nm) which Gaussian fits a single unique observed absorption line, in this cases I discard all the atomic lines except the one with the greatest theoretical equivalent width (i.e., this one has the higher probabilities to be the main contributor to the observed line). From this process, a total of 2496 atomic lines were selected.

3.5.2 Deriving solar abundances

The second step is to determine abundances with all the codes and methods for each of the selected lines in the solar spectrum by fixing the following reference solar parameters (based on the Gaia Benchmark Stars recommended values):

- Effective temperature (T_{eff}): 5771 K
- Surface gravity ($\log(g)$): 4.44 dex
- Metallicity ($[M/H]$): 0.00 dex
- Microturbulence velocity (V_{mic}): 1.07 km/s
- Macroturbulence velocity (V_{mac}): 4.21 km/s
- Projected rotational velocity ($v \sin(i)$): 1.60 km/s
- Limb darkening coefficient: 0.6

I used solar abundances from [Grevesse et al. \(2007\)](#) to be consistent with MARCS model atmosphere. The macroturbulence broadening is implemented using the radial-tangential formalism as described in [Niemczura et al. \(2014\)](#) (adapted from SME), and the projected rotational velocity plus the limb darkening coefficient are applied following Eq. 17.12 from [Gray \(2008\)](#) (adapted from SYNSPEC, [Hubeny & Lanz \(2011\)](#)). All these effects are directly implemented into iSpec and are applied independently of what was the selected radiative transfer code.

3.5.3 Equivalent width

Using MOOG and WIDTH9 radiative transfer codes, I determined the abundances for all the selected lines using the equivalent width (EW) derived from the previously fitted Gaussian profiles. Additionally, to be able to assess the quality of each line I also derived abundances when the metallicity is artificially increased by 0.10 dex (assessing the impact when there are errors in the metallicity) and abundances when the EW is drawn from a random distribution using the fitted EW as the mean and its error (computed following [Vollmann & Eversberg \(2006\)](#)) as the sigma (testing signal-to-noise ratio influence).

3.5.4 Synthetic spectral fitting technique when interpolating model atmospheres

In this method the codes SPECTRUM, Turbospectrum, SME, MOOG and SYNTH are used. For each line, I first compute a small synthetic spectrum that includes the target line and I use it to adjust the line mask (spectral region used by the minimization algorithm), this way if close-by lines are present in the synthetic spectra but not in the observed one, their impact can be reduced by excluding it from the mask. I cross-correlate the same synthetic spectrum with the observed one to detect and correct small line

shifts. Then, the abundances are determined by letting free only the corresponding element. To later assess the quality of each line (i.e., filtering out lines with differences larger than certain limits), I also derive abundances for that line when the metallicity is artificially increased by 0.10 dex, when a new realisation of the spectrum is created (fluxes are drawn from a poisson distribution using the fluxes as mean values and errors as the sigma) and when the atomic line list only contains the target atomic data and not any other blended line.

3.5.5 Synthetic spectral fitting technique when interpolating pre-computed spectra

In the previous two methods, iSpec interpolated model atmospheres using the MARCS grid and provided it to the corresponding radiative transfer code. In this method the atmospheres are not interpolated, but a grid of synthetic spectra was pre-computed using SPECTRUM and matching the exact atmospheric parameters that the MARCS grid provides but with two different alpha abundance variations ($[\alpha/\text{Fe}] = \pm 0.40$ dex, where alpha elements correspond to Neon, Magnesium, Silicon, Sulfur, Argon, Calcium, and Titanium) and four microturbulences (0.00, 1.00, 2.00 and 4.00 km/s). Thus, the dimensions of the grid are effective temperature, surface gravity, metallicity, alpha enhancement and microturbulence. The grid is computed with a very high resolution ($R > 300\,000$), this allows iSpec to interpolate a very high-resolution spectrum that can be then degraded to the target resolution and effects such as macroturbulence, rotation and limb darkening can be applied.

For each line, I perform the same radial velocity correction as explained in the previous section and I derive the abundance for each line. In this case, I set free the metallicity parameter since the grid does not have a dimension for every possible chemical element. This strategy is also followed by other authors and surveys (e.g., APOGEE) when using pre-computed grids. To be able to assess the quality of the line, an abundance is also derived for a new realisation of the spectrum (as explained in the previous section).

3.5.6 Selecting lines

I created two line selections for each code: one optimized to be used for determining atmospheric parameters and a second less strict one that can be used for a line-by-line determination of individual chemical abundances. To make these line selections, I defined the following simple criteria to evaluate if an absorption line should be selected: a line can be considered good when I am able to derive an accurate solar abundance. In practice this means that the derived abundance respect to the solar abundance of reference (understood as $[X/H]$) should be close to zero within a certain margin.

After several tests, I found that the optimal margin for the determination of atmospheric parameters with equivalent width methods is ± 0.10 dex (enough neutral and ionized iron lines need to pass this filter), while for the synthetic spectral fitting technique the margin can be of ± 0.05 dex. For the former, only iron lines are considered while for the latter, I consider only lines not affected by hyperfine struc-

ture splitting and that proxy iron peak (Iron, Chromium, Nickel) and alpha elements (Silicon, Calcium, Titanium).

It is worth noting that these selected lines will not be blindly used with all the target spectra. Before executing the determination of atmospheric parameters, I fit Gaussian profiles to all the selected lines using the target spectrum and I discard those that do not contain valid fluxes, are affected by telluric lines, have a bad line mask, the Gaussian profile fit failed or has a too large root mean square (i.e., RMS error ≥ 1.00), has a reduced equivalent width greater than -4.2 or lower than -6 (to avoid saturated or too weak lines), or has an excitation potential too extreme (e.g., greater than 6 eV, where there are almost no lines and an outlier can deeply affect trend computations). Hence, the line selection will be further fine-tuned and adapted to each target spectrum to be analysed.

Once the atmospheric parameter of a star are found, the determination of individual chemical abundances can be calculated differentially line-by-line and it is not necessary to be so strict with the selection criteria, especially if we want to include certain elements that have only a few difficult lines. Thus, if an element has more than ten lines, the strict margin is applied (± 0.10 and ± 0.05 dex for equivalent width and synthesis, respectively) but if not, a more generous margin of ± 0.50 dex is enforced (value also determined from experimental tests). With this strategy, we can maximize the number of elements for which we can derive abundances without affecting the quality of the elements that already have many lines.

Some more quality controls are applied to the line selection for atmospheric parameters and the line selection for individual chemical abundances. Absorption lines close to the known strong lines H- α (652 - 660 nm), H- β (483.5 - 489.5 nm) and Mg triplet (514 - 521 nm) are discarded. Weak lines are more impacted by continuum placement, to reduce this effect I discard absorption lines with depth lower than 0.05. The determination of line shifts can go wrong for very weak and noisy lines or extremely blended lines, based on some manual tests the best indicator to identify this cases is the error on the radial velocity that comes from the cross-correlation process which should be lower than 100 km/s (from visual inspection, errors larger than this are correlated with problematic lines while slightly lower errors can be due to problematic lines or overestimated errors). Abundance errors are also good indicators to identify good fits, I discard any line with an error greater than 0.25 dex. Abundances derived from new realisations of the equivalent width or the spectrum fluxes should not be more than 0.10 dex away from the main derived abundance, otherwise the line is too sensitive to the noise. Finally, only for synthetic spectral fitting technique using atmospheric model interpolation, I discard lines with abundances more different than 0.10 dex when the metallicity has been artificially set 0.10 dex higher, and lines which abundance is 0.50 dex different when using atomic line list without blended lines.

3.6 Atmospheric parameters and abundances

The determination of parameters can take place in one or two full iterations depending on how we want to normalize the spectra (each full iteration includes a normalization and the determination of parameters executed by the min-

imization algorithm which goes through multiple iterations exploring the parameter space until converge). The first full iteration will normalize the spectra (before deriving any parameter) by applying a median and a maximum filter with different window steps (0.05 and 1.0 nm, respectively) and fitting the continuum with a B-spline of 2 degrees every 5 nm (ignoring automatically detected strong lines by iSpec). It is worth noting that the same normalization process was used in the line selection described in Sect. 3.5. The second full iteration, if enabled, will synthesize a spectrum (i.e., template) with the atmospheric parameters found in the first full iteration, the observed spectrum is divided by the template and I apply median and Gaussian filters with different window steps (0.05 and 10 nm, respectively) to find the continuum. The advantage of using a synthetic spectrum as a template is that areas with strong lines and many blended lines (e.g., the blue part of the visual range for cooler stars tends to be very crowded and blended) will be better normalized and differences between spectra from the same star but with different noise levels will be normalized more similarly, hence the determination of parameters in that second full iteration may improve with respect to the first full iteration. The risks are that the first full iteration may already lead to inaccurate parameters (i.e., the template will be synthesized with bad parameters) and lines existing in the synthetic spectrum but not in the observed one can create normalization artefacts.

To accelerate the convergence process during the determination of atmospheric parameters, it is optimal to start with initial parameters as close as possible to the type of star we are analysing. I pre-computed with each code a very limited grid of synthetic spectra which only covers four temperatures (3500, 4500, 5500 and 6500 K), two surface gravities (1.5 and 4.5 dex) and three metallicities (-2.0, -1.0 and 0.0 dex). The normalized observed spectrum is compared to all the spectra in the grid and the parameters of the one with the lowest χ^2 are selected as initial values. This process allows me to quickly distinguish between metal-poor/rich dwarfs and giants and start the minimization algorithm with values closer to the final solution, speeding up the converge.

For the equivalent width method, iSpec lets effective temperature, surface gravity and/or microturbulence velocity to be set-up as free parameters and a maximum of twenty iterations are allowed. While for the synthetic spectral fitting technique use the effective temperature, surface gravity, metallicity, alpha enhancement, microturbulence velocity and resolution as free parameters with a maximum of six iterations (several tests showed these are reasonable maximums to obtain accurate results in an optimal computation time, see Blanco-Cuaresma et al. (2014b)). The resolution, macro-turbulence and projected rotational velocity are degenerated parameters which are very difficult to disentangle by only relying on spectroscopy. After several tests, the most accurate results were obtained when we absorb macro-turbulence, rotation and resolution variations by setting only the resolution as a free parameter while rotation is fixed to 1.6 km/s and macro-turbulence follows an empirical relation established by GES considering the effective temperatures, surface gravities and metallicities from their dataset (although setting this parameter to zero also leads to similar results).

The determination of individual chemical abundances follows the same structure described in Sect. 3.5.2 where

individual line shifts are detected by cross-correlating the spectrum region of the target line with a synthetic template, then abundances are derived using the corresponding method and some additionally controls are executed as explained in Sect. 3.5.3, 3.5.4 and 3.5.5. I discard lines for which it was not possible to derive the main abundance or any of the quality control abundances, and lines with extreme abundances that fall outside the metallicity range considered by the atmospheric models grid (i.e., abundances with respect to the Sun greater/lower than 1.0/-5.0 dex). From the remaining dataset, I discard lines that do not pass the quality controls following the same criteria explained in Sect. 3.5.6 except for elements which only have one line (I relax the criteria to maximize the number of measured elements).

To partially compensate modelling errors, it is preferable to perform a differential abundance analysis. For certain studies it could be convenient to use more than one reference star in different evolutionary stages (Blanco-Cuaresma & Fraix-Burnet 2018; Blanco-Cuaresma & Soubiran 2016), but for this work I used the Sun as only reference and I included seven solar spectra from the Gaia Benchmark Stars library which were analysed using the same process as for the rest of the spectra (i.e., pre-processing, normalization, atmospheric parameters and abundances determination). For most of the selected lines I get seven different measurements (one per spectrum) that I use them to compute an averaged abundance and a dispersion (to be used as error). To ensure good reference values I filter lines that were not measured in more than three solar spectra (some lines can fail due to quality issues in the observed spectrum or missing fluxes). For the rest of stars, the final differential abundances are derived by subtracting the reference abundance line by line, while errors are added quadratically.

3.7 The non-observed dataset experiment

As described in Sect 2, the main analysis in this work uses the high-resolution spectra from the Gaia FGKM Benchmark Star public library. Observed data may be affected by many different variables that depend on the instrument used, the night conditions, the treatment of the raw data, etc. Additionally, there is no model that can perfectly reproduce all the physical processes that take place in a star (e.g., theoretical assumptions are done to make the problem approachable with our current computer resources and time constraints). To discard that any of these variables is playing a role in the main analysis done in this work, I created a purely theoretical dataset by synthesizing spectra using the Gaia FGKM Benchmark Star reference values, the signal-to-noise ratios from the public library, and all the synthesis codes used in this study plus the interpolation from a pre-computed grid method. This produced a dataset of 672 normalized synthetic spectra, which has been analysed following the same procedure as the observed dataset.

3.8 The one variable at a time experiment

To understand what each code does and how they differ in detail, there are mainly two broad strategies: 1) Read the documentation, ask the author(s) and invest a large amount

of time interpreting the thousands of lines present in each source code (if available); 2) Design an experiment where one output variable is measured while all the input variable remain constant except one. These are not exclusive strategies, following both of them would be instructive but given the complexity of the codes (also written in different programming languages, and one of them not being public) and the limited amount of resources, I mainly followed the second one.

In the case of the equivalent width method, I consider the lines in common between both codes (MOOG EW and WIDTH) plus the equivalent widths measured in the same solar spectrum used in Sect. 3.5, and I measure the median abundance. In the case of the spectral fitting technique, I do not use any observed data and I measure the synthetic flux depth around 556.45 nm (a region with practically no blend, thus close to the continuum) and the flux depth at the line peaks for the common selection. In both cases I use the solar parameters shown in Sect. 3.5.2, all the default values for the atomic line list and atmospheric model, and the results from MOOG (EW) and SPECTRUM, respectively, as reference point.

In the experiment, I track the changes to the reference equivalent width abundance, continuum and absorption line peak depths while 1) changing (one at a time) the effective temperature, surface gravity, metallicity, alpha enhancement, microturbulence, number of layers in the atmospheric model; 2) multiplying by a factor (between 0.25 and 1.75) the values of column mass (ρ_{ox}), temperature, gas pressure (p_{gas}), electron density (x_{ne}), Rosseland mean absorption coefficient (abross), radiation pressure (accrad), microturbulence velocity (v_{turb}), optical depth ($\log\tau_5$) and electro pressure (p_{electron}) on each atmospheric model layer; 3) multiplying by a factor (between 0.25 and 1.75) the values of oscillator strength ($\log gf$), radiative damping parameter (rad), stark damping parameter (stark), van der Waals damping parameter (waals). The factor multiplication was applied as a logarithmic addition for parameters expressed in logarithmic terms such as $\log\tau_5$, $\log gf$, rad , stark and waals .

4 RESULTS

4.1 Line selection

The total number of selected lines for each code (as described in Sect. 3.5) are shown in the diagonal of the table drawn in Figure 1, the rest of the table shows the number of lines in common between each pair of codes. MOOG EW (i.e., MOOG using equivalent width) is the code with which the greatest number of accurate solar abundances were obtained, followed by Grid (synthetic spectral fitting using a grid of pre-computed spectra with SPECTRUM) and SYNTH. As a reminder, lines from the equivalent width codes were selected using a looser criteria than the rest (as described in Sect. 3.5.6) and these numbers are not directly comparable.

Only by looking at the colour coding of the results we can notice two separated islands: equivalent width codes (MOOG EW and WIDTH9) and synthesis (Grid, SPECTRUM, Turbospectrum, SME, MOOG Synth and SYNTH). They have a greater number of lines in common

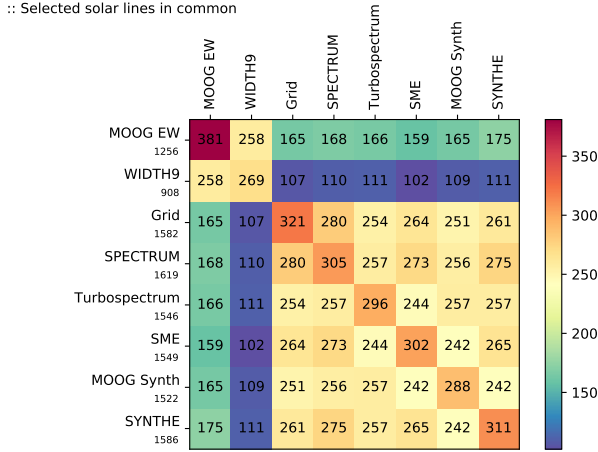


Figure 1. Absorption lines in common for which a ± 0.05 dex abundance (± 0.10 for MOOG EW and WIDTH9) was derived with a particular code when analysing the NARVAL solar spectrum with highest signal-to-noise ratio. The number below each code name correspond to the sum of all the values in the row minus the lines that correspond to the same code. The label Grid corresponds to the results obtained when interpolating from a pre-computed grid of synthetic spectra.

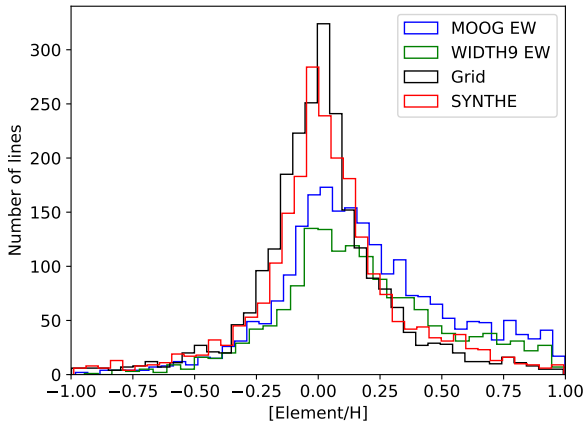


Figure 2. Original distribution of derived abundances for the solar spectrum before any filtering was applied.

within themselves but not so many across each other, this can be intrinsic to how these methods work: one only considers the area of an absorption line, while the other takes into account the full shape of the line profile including blends (see also Sect. 5.1 in Casamiquela et al. 2017). When comparing line-by-line abundances for each element from the two methods, we can observe that the equivalent width method provides bigger abundances than synthesis since the latter can reproduce and account for blends (if I force the synthesis to ignore blends, the agreement with equivalent width results increases as shown in Sect. 5.1 in Casamiquela et al. 2017). At the same time, saturated lines (those with a greater reduced equivalent width) depart from a Gaus-

sian profile (used to determine the equivalent width) and the equivalent width method derives smaller abundances. The example shown in Figure 3 compares codes that use the same radiative transfer core code, thus these differences do not arise from major differences in their implementations but from the intrinsic differences between the two methods.

In a previous discarded analysis (not included in this work), when interpolating from a grid of spectra that was computed with only two microturbulences (0.00 and 4.00 km/s), a lower number of lines in common with pure synthesis was found. Hence, increasing the number of data points to cover four microturbulences (0.00, 1.00, 2.00, and 4.00 km/s) led to a higher agreement between grid and the rest of synthesis codes.

A line-by-line comparison between Grid and SPECTRUM (the code used to pre-compute the grid) shows no systematics for any particular element (see Figure 4). When comparing line-by-line equivalent width code results, some systematics are observed for certain elements and major disagreements appear with larger reduced equivalent widths (see Figure 5). Similar systematics are also observed for synthesis codes, but the size of the reduced equivalent width does not seem to have any major impact on the results between different codes (see Figures 6 and 7). This shows the importance of executing line-by-line differential analysis to minimize different systematics between codes.

In total, considering the abundances within ± 0.05 dex with respect to the solar abundance, there are only 45 absorption lines in common between all the codes (of which 26 correspond to neutral iron, one to ionized iron). It would not be possible to determine atmospheric parameters with these limited number of lines. Instead, given the different nature of the equivalent width method and the synthetic spectral technique, I created one line selection for each approach (hereafter, the common line selection). The common line selection is composed of 258 lines (where 146 correspond to neutral iron and 11 to ionized iron) for equivalent width methods (i.e., MOOG EW and WIDTH9), and 205 lines for Grid plus the rest of synthesis codes. The numbers are higher for the former because a less strict limit was required for this method (i.e., the limit was set to ± 0.10 instead of 0.05 as explained in Sect. 3.5.6, otherwise not enough ionized iron lines would be left).

Regarding lines selected for chemical abundance determination where the constraint were more relaxed as described in Sect. 3.5.6, an average of ~ 1200 lines were selected for all the codes with the exception of WIDTH9 and Grid for which ~ 900 and ~ 1400 lines were selected. This is coherent with the original distribution of derived abundances shown in Figure 2, where WIDTH9 underperforms compared to MOOG EW, equivalent width codes show a larger variance with a skewed distribution favouring bigger abundances and Grid has the largest number of lines around zero.

4.2 Impact on atmospheric parameters

4.2.1 Full Gaia Benchmark Stars dataset

Using the common line selection, I compare the derived atmospheric parameters for the Gaia Benchmark Stars by computing the mean difference between each radiative trans-

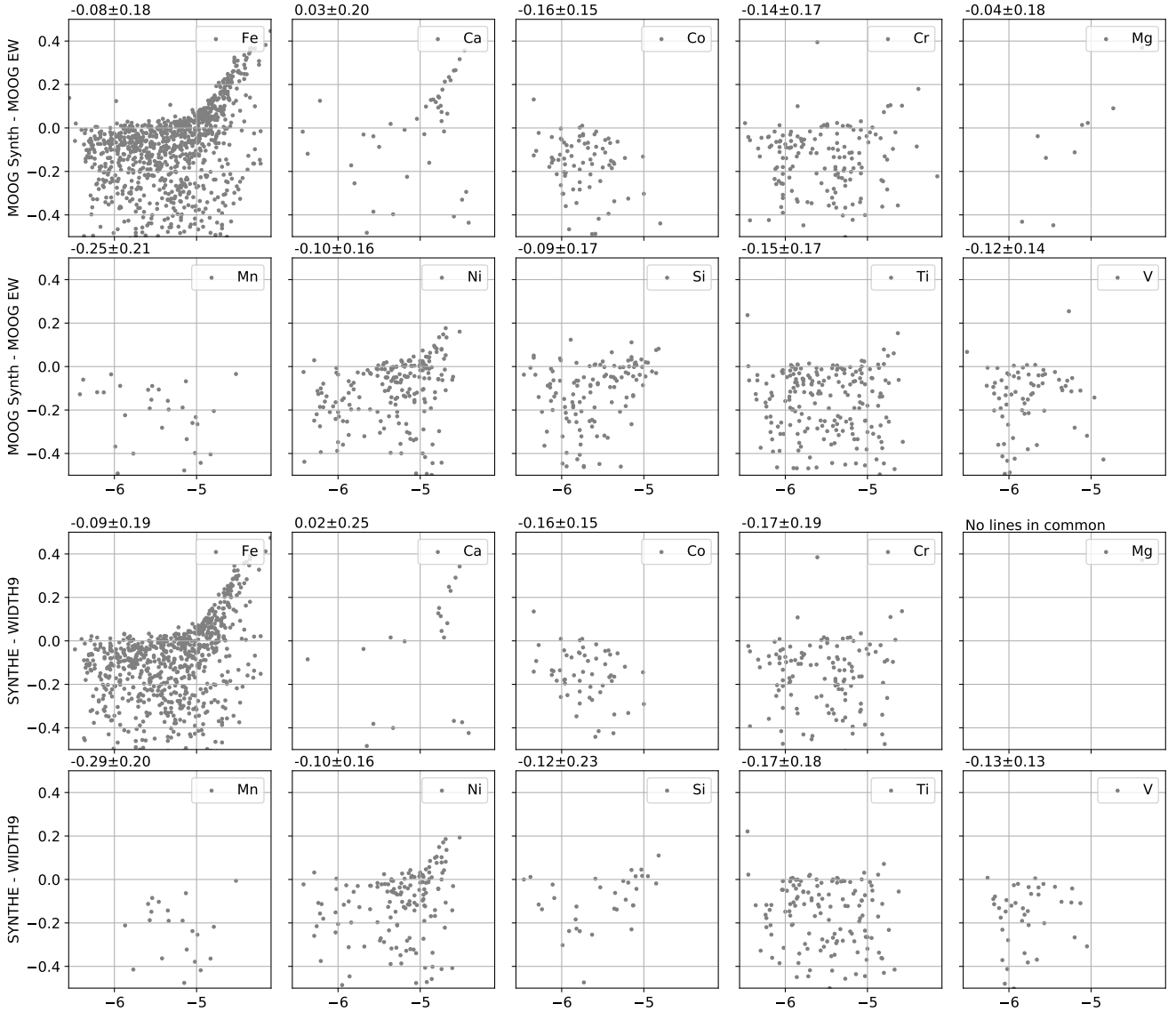


Figure 3. Solar abundance difference between equivalent width and synthesis codes as a function of reduced equivalent width for different elements. Median and absolute median deviation are indicated on the upper left of each subplot.

fer code and calculating the robust standard deviation¹⁰ (i.e., dispersion) of these differences in Figure 8. Ideally we would like both quantities to be as close as possible to zero, meaning that the precision is high between different pairs of radiative transfer codes. The dispersion found in the three atmospheric parameters shows again two islands that separate equivalent width methods from synthesis with precisions higher within each group but not the two groups.

In terms of median differences, a clear bias is observed for the surface gravity and a less significant systematic in effective temperature where the equivalent width methods

provide consistently higher and lower values, respectively. This effect may be driven by the differences in the microturbulence velocity as shown in Figure 9. The microturbulence parameter represents ensemble velocity fields that are not available in 1D model atmospheres (in 3D models this parameter is not necessary), and these velocity fields have broadening effects (depth-independent) on the line opacity (it serves to desaturate the line). The differences shown for the microturbulence velocity, especially between the equivalent width method and the synthetic spectral fitting technique, could be due to a compensatory effect on differences in the derived effective temperatures and surface gravities or to real differences between methods and codes. The latter is explored with the experiment described in Sect. 3.8, which results are presented in Sect. 4.5.

To be able to visually compare all the parameters for all

¹⁰ Function `mad_std` from the `astropy.stats` package (The Astropy Collaboration et al. 2018; Astropy Collaboration et al. 2013): $\sigma \approx \frac{\text{MAD}}{\Phi^{-1}(3/4)} \approx 1.4826 \text{ MAD}$ where $\Phi^{-1}(P)$ is the normal inverse cumulative distribution function evaluated at probability $P = 3/4$

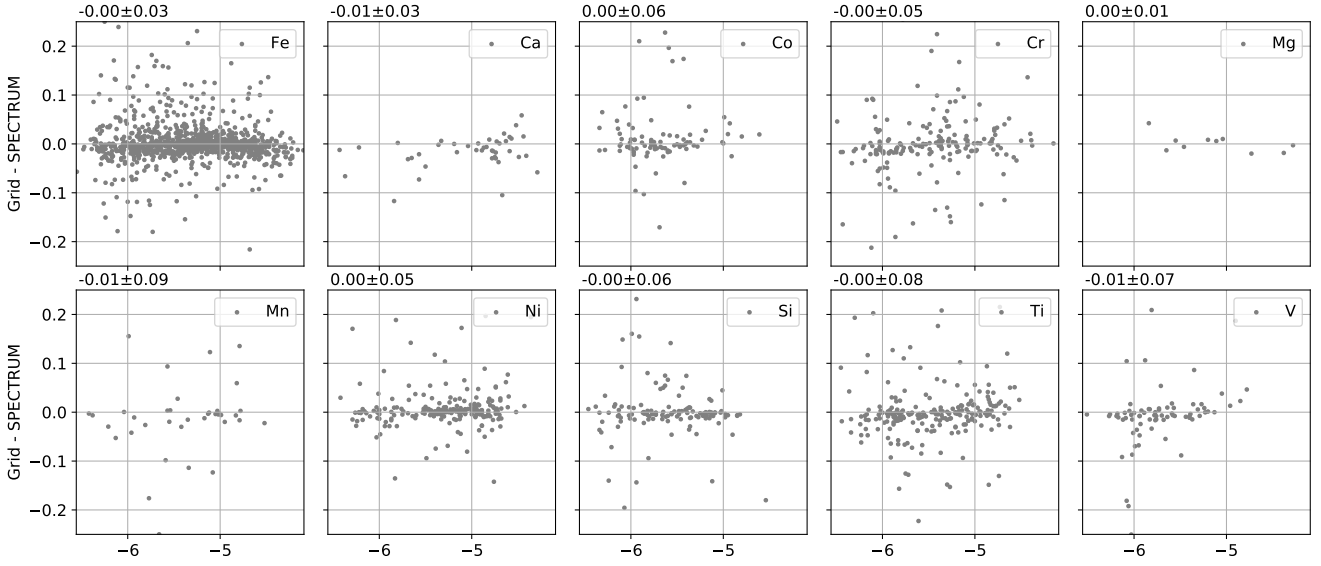


Figure 4. Solar abundance difference between synthesis and interpolation from pre-computed grid of spectra (i.e., Grid) as a function of reduced equivalent width for different elements. Median and absolute median deviation are indicated on the upper left of each subplot.

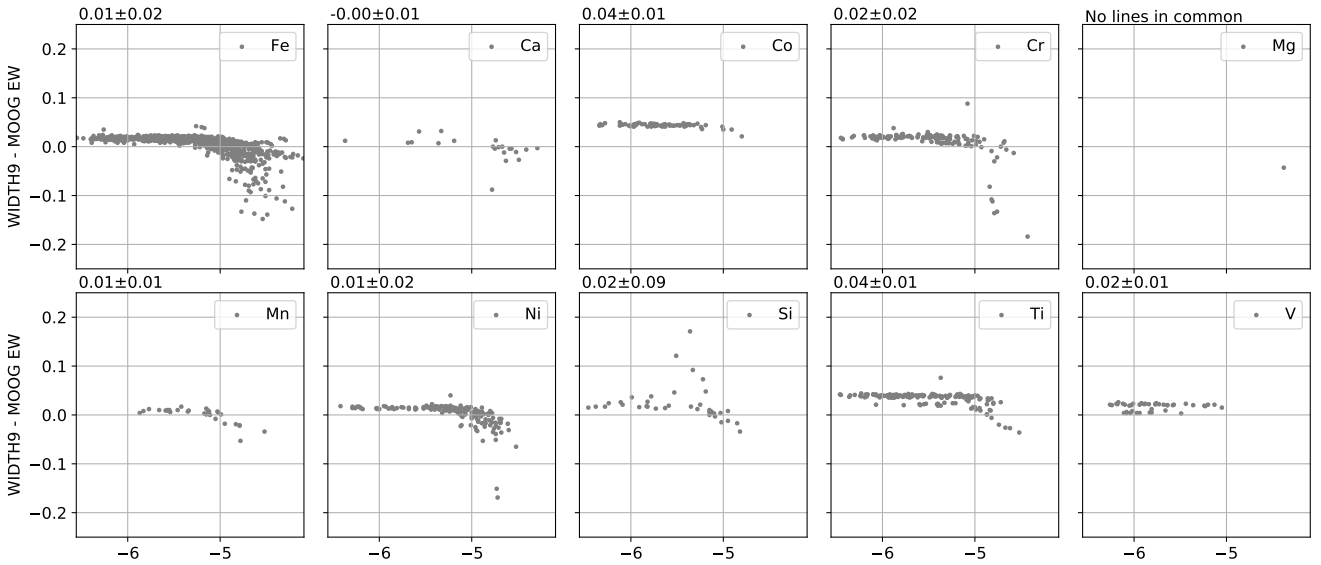


Figure 5. Solar abundance difference between equivalent width codes as a function of reduced equivalent width for different elements. Median and absolute median deviation are indicated on the upper left of each subplot.

radiative transfer codes at the same time, I normalized¹¹ all the values from Figure 8 and added them together as shown in Figure 10 (left plot). Additionally, I repeated the same operation for all the results obtained when the best line selection (hereafter also, the own lines selection) for each code is used (right plot). Using the best line selection improves the statistics by increasing the number of lines but it also

introduces more inhomogeneities in the analysis. The former effect dominated for synthesis codes since the agreement among them slightly increased (mainly for MOOG Synth), while the latter was more significant for equivalent width methods where WIDTH9 results separated from MOOG and it slightly leaned towards synthesis.

Assessing the precision between pairs of codes allow us to verify what codes lead to the most similar results but does not verify which code and/or set-up is obtaining the closest results to the expected reference parameters (e.g., two codes may be very imprecise because only one of them is very accurate). The accuracy of the results (difference respect

¹¹ All the values were scaled to unit norm (vector length) using the `sklearn.preprocessing.normalize` function (Buitinck et al. 2013; Pedregosa et al. 2011).

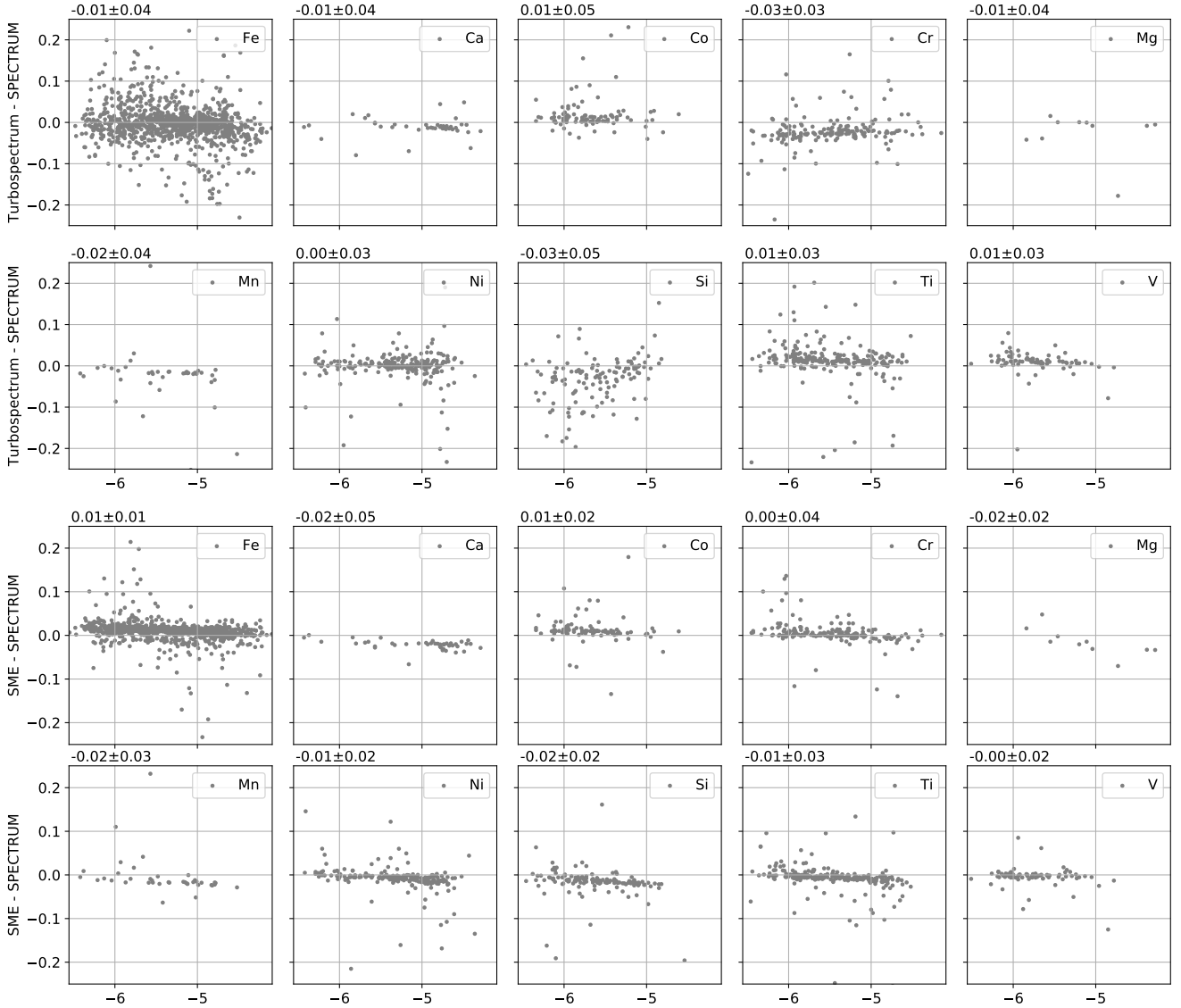


Figure 6. Solar abundance difference between synthesis codes as a function of reduced equivalent width for different elements. Median and absolute median deviation are indicated on the upper left of each subplot.

to the Gaia Benchmark Stars reference values) is shown in Figure 11. I run the analysis with eight different setups using the selection of common lines or the best lines for each code plus enabling/disabling the following options:

- In addition to the selected lines, consider the wings of H- α / β and Mg triplet. Enabling this option is not possible for the equivalent width methods, for which the same results are just duplicated in Figure 11.
- Run a second full iteration as described in Sect. 3.6, where the normalization is repeated but using a synthetic spectrum as a template (which matches the atmospheric parameters found in a first full iteration) and re-determine the atmospheric parameters again.

The equivalent width method presents a higher dispersion for all the atmospheric parameters. It also has the lowest level of agreement when analysing several spectrum corre-

sponding to the same star as shown in Figure 12. Metallicity is not included in that figure because results are very similar across codes, the median robust standard deviation per star is around 0.03 dex for equivalent width methods and 0.01 dex for synthesis. The synthetic spectral fitting technique performs better in this test mainly because the Gaia Benchmark Stars includes a wide range of FGKM stars and the equivalent width method is not the best option for all of them (see Sect. 4.2.2). For instance, the accuracy of the equivalent width method degrades more strongly with cooler stars due to blends and metal poor stars due to lack of iron lines.

To visually compare all the parameters for all radiative transfer codes and setups at the same time, I normalized and added all the values from Figures 11 and 12 as shown in Figure 13. As general rule, using the best line selection instead of the common line selection leads to better accu-

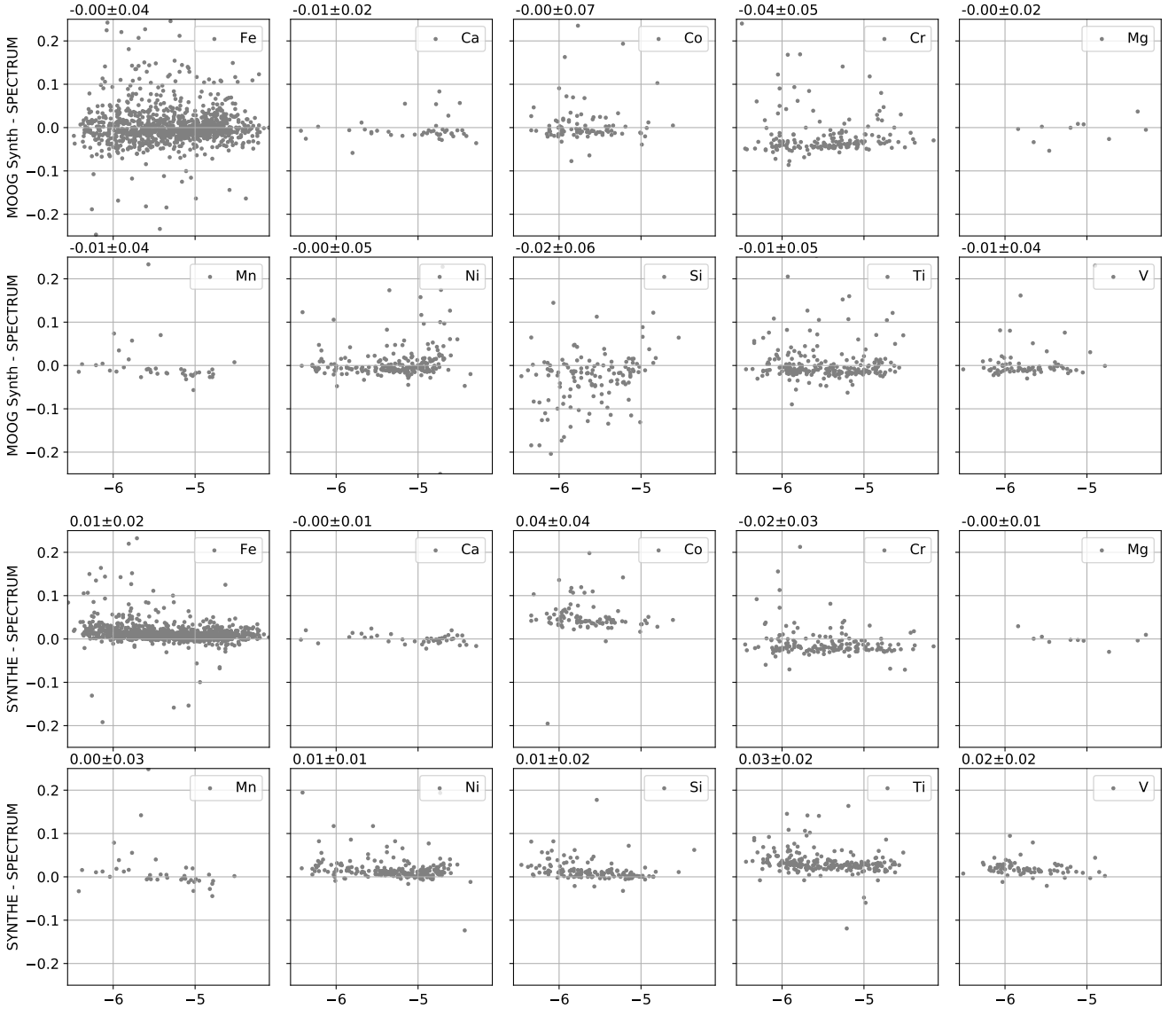


Figure 7. Same as in Figure 6

racy for all the codes thanks to the increase in the statistics without sacrificing quality.

The codes MOOG EW and WIDTH lead to similar results for the equivalent width method, being MOOG EW the best of both when using its own line selection and executing a second full iteration normalising with a synthetic spectrum matching the atmospheric parameters found in the first full iteration. This second full iteration does not have the same positive effect for all the codes. Its major contribution is improving the dispersion per star for most synthesis codes as shown in Figure 12, but sometimes it slightly worsens the overall results. The effect of this second full iteration could be due to the template based normalization or due to the execution of an extra batch of iterations until convergence for determination of atmospheric parameters is reached. I executed a validation test with Grid using only one full iteration with the best line selection but allowing the process that determines the atmospheric parameter to run for a higher

maximum number of iterations (twelve instead of six), and the results did not change significantly (RMS decreased by less than 0.01 for eleven spectra, the rest remained at the roughly the same level). This is a strong indication that the effects of adding the second full iteration are mainly due to the template based normalization.

For the synthetic spectral fitting methods, adding the wings of H- α/β and Mg triplet generally improves the results for Grid, SPECTRUM and SYNTHES, while it worsens the results for Turbospectrum, SME and MOOG Synth. To rule out that the normalization process is not favoring some of the codes, a comparison of an observed NARVAL solar spectrum and an observed solar ATLAS (Hinkle et al. 2000) is shown in the top subplots of Figure 14 where the agreement is outstanding. Synthetic solar spectra for each code is also shown on the bottom subplots of the same figure, SME and Turbospectrum are close together on the deepest end while MOOG is on the other extreme. Grid, SPECTRUM

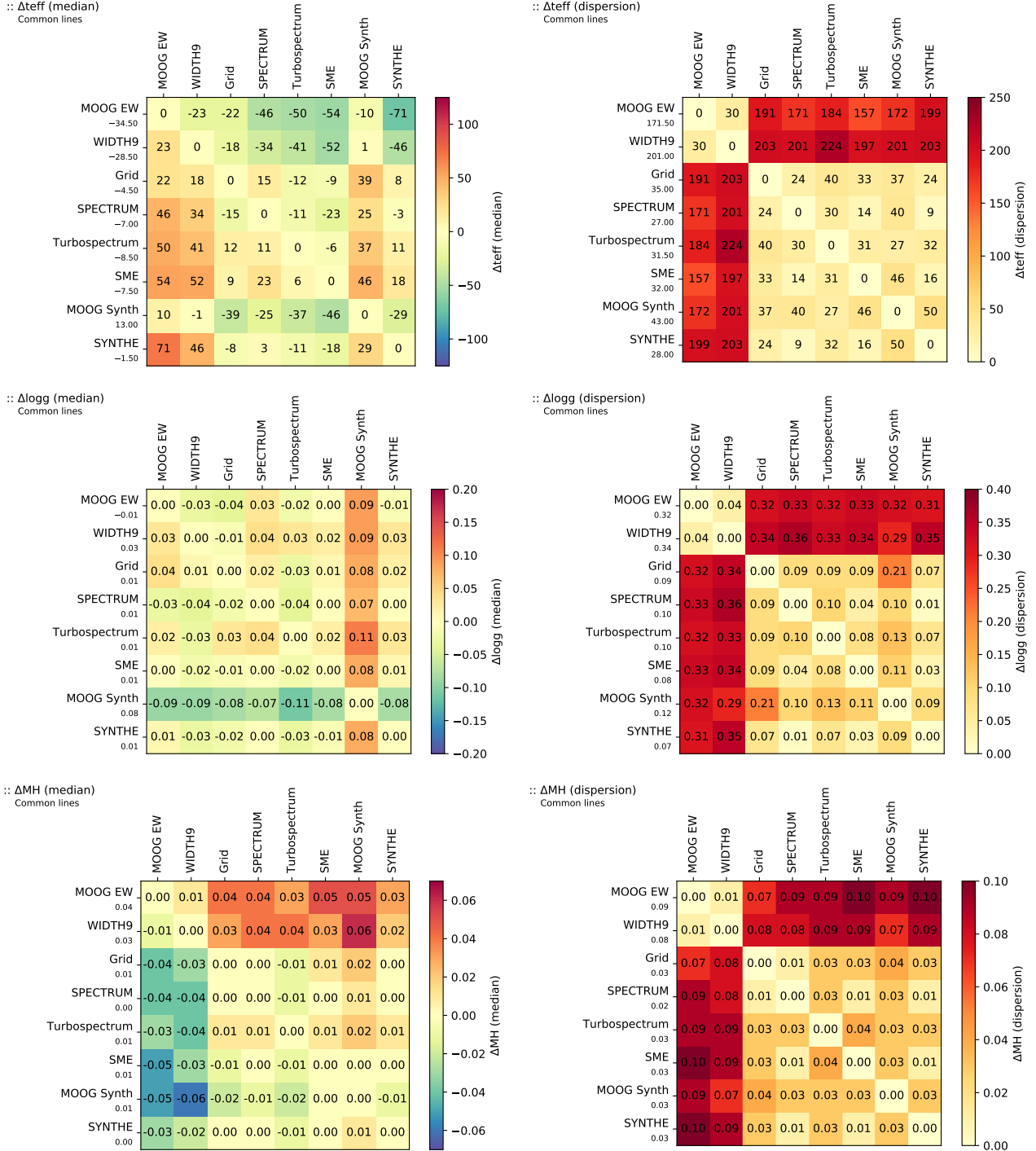


Figure 8. Median and robust standard deviation of the difference in effective temperature, surface gravity or metallicity between different radiative transfer codes when analysing the Gaia Benchmark Stars and using the common line selection (subtraction sense: row minus column).

and SYNTH strongly overlap with each other and they are generally closer to the observed spectrum. These discrepancies reflect differences in how the broadening of the hydrogen lines are computed by each code.

Determining effective temperatures using the wings of the hydrogen lines is a known strategy (Niemczura et al. 2014; Cayrel et al. 2011) which is understood to be very dif-

ficult (Barklem et al. 2002). In this context, Giribaldi et al. (2018) shows how normalization plays a major role and they identify a systematic of 28K for the Sun when using H- α . Given the differences found in this work for the considered radiative transfer codes, I executed an extra analysis where I determine the effective temperature for all the Gaia Benchmark Stars using the wings of H- α and H- β separately and

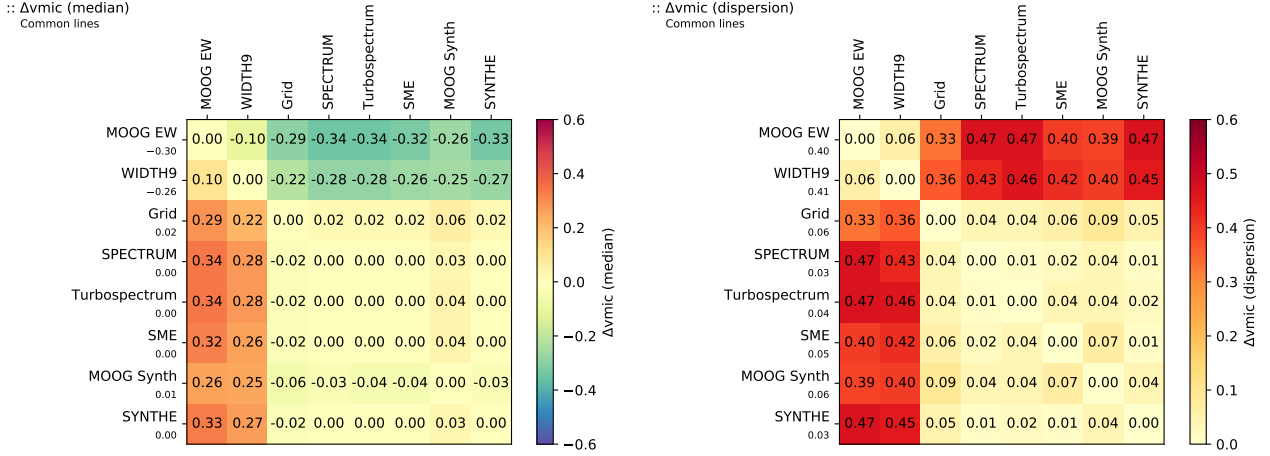


Figure 9. Median and robust standard deviation of the difference in microturbulence velocity between different radiative transfer codes when analysing the Gaia Benchmark Stars and using one common line selection for equivalent width methods plus another common one for synthetic spectral fitting technique.

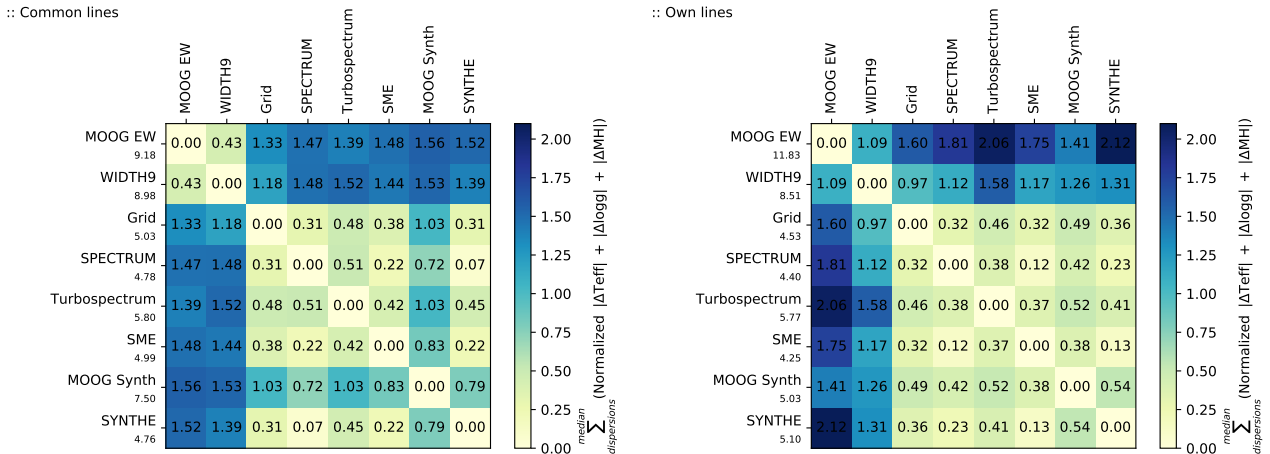


Figure 10. Sum of the normalized absolute median differences with respect to other codes, normalized robust standard deviation for effective temperature, surface gravity and metallicity when analysing the Gaia Benchmark Stars. Lower numbers indicate the codes lead to more similar results (higher precision).

	Grid	SPECTRUM	Turbo.	SME	MOOG	SYNTH
H- α	-30 \pm 27	-6 \pm 30	-105 \pm 29	-138 \pm 26	239 \pm 22	-21 \pm 31
H- β	-93 \pm 45	-79 \pm 46	-185 \pm 46	-237 \pm 49	367 \pm 85	-87 \pm 46
H- α +H- β	-217 \pm 69	-185 \pm 69	-322 \pm 65	-381 \pm 59	795 \pm 128	-188 \pm 71

Table 2. Median and absolute median deviation for differences between effective temperatures derived using the wings of hydrogen lines and the solar reference value.

together, while the rest of parameters are fixed to their value of reference. The results are shown in Figure 15. H- β is the worse modelled line of the two as shown in the middle subplots, however, when combined with H- α (right subplots) the results improve for most of the codes except MOOG. Turbospectrum, SME and MOOG show the largest systematics and this may be the reason why these adding these regions to the different analysis presented in this work do

not improve the overall results. If I limit the validation to the solar spectra, the closest effective temperature to the reference value is obtained when using only H- α with Grid, SPECTRUM and SYNTH as shown in Table 2.

The best global results (i.e. considering all the methods/codes) are obtained using each code's own line selection. I used these results to assess the accuracy and precision in function of effective temperature, surface gravity and metallicity. Figures 16 and 17 illustrate accuracies by comparing the results to the reference values, and they show that the biggest disagreements tend to happen with cold and/or metal poor stars, especially significant for the equivalent width method as explained in the next section. In terms of agreement between the two equivalent width codes (see left subplots in Figure 18), discrepancies seem to be fundamentally influenced by the stellar metallicity although higher discrepancies also appear for lower and higher effective temperatures and surface gravities. Metallicity also affects the level of agreement between synthetic spectral fitting codes

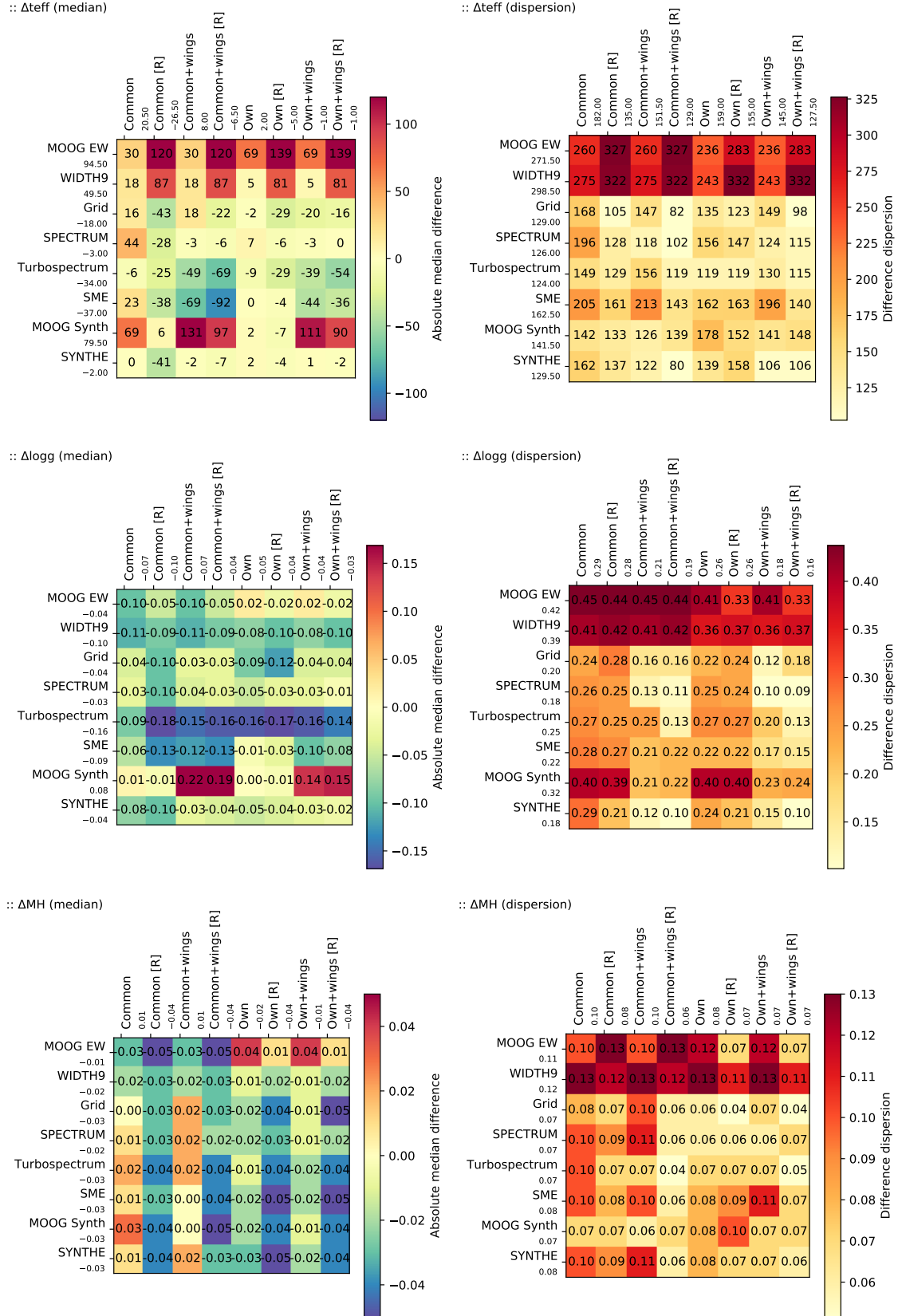


Figure 11. Median and robust standard deviation of the difference in effective temperature with respect to the reference values when analysing the Gaia Benchmark Stars and using different radiative transfer codes with several setups: using lines in common within equivalent width and synthesis methods (labelled as "Common"), using the best lines for each code (i.e. their own lines, not necessarily good for other codes; labelled as "Own"), using the wings of H- α/β and Mg triplet (labelled as "Wings"), repeating the normalization (labelled as "[R]") but using a synthetic spectrum that matches the atmospheric parameters found in the first iteration.

(see Figure 19), certain code pairs also show higher disagreements for giant stars and the coolest star. When one code from each method is compared as shown on the right subplots in Figure 18, the highest discrepancies are found for stars with low temperatures, gravities or metallicities.

4.2.2 Limited Gaia Benchmark Stars dataset

The accuracy of the equivalent width method can be affected by the presence of strongly blended lines and by the lack of enough observed iron lines, while the synthetic spectral fitting technique is more lenient. Hence, the cooler and/or more metal poor Gaia Benchmark Stars are challenging targets for the equivalent width method and to account for this, I repeated the previous assessment but selecting only the derived atmospheric parameters for the Gaia Benchmark Stars that have a reference effective temperature greater than 4500 K and a metallicity higher than -1.0 dex. In Figure 20, I show the added normalized median differences and robust standard deviation between codes (i.e., precision) using the common and their own line selections. Interestingly, the similarities between codes are in line to what it was observed in Figure 10, but in this case is MOOG EW which gets closer to synthesis codes when using their own line selection instead of WIDTH9.

Regarding the accuracy of the codes depending on their set-up, Figure 21 shows a similar patterns to Figure 13 except that the equivalent width results significantly improve and become more competent when this limited subset of the Gaia Benchmark Stars are considered, being MOOG EW the best code for equivalent width.

4.3 Impact on chemical abundances

4.3.1 Full Gaia Benchmark Stars dataset

Individual chemical abundances were derived fixing the atmospheric parameters to the reference values and using the best line selection for each method. The iron abundances tends to be used as a proxy for metallicity, and indeed Figure 22 shows very similar patterns to Figure 8 (bottom plot) where equivalent width codes and synthesis form separate islands. However, the dispersion is worse in Figure 22 for the equivalent width codes. Imposing the same atmospheric parameters to all the spectra most probably worsen the results because, as shown in Sect 4.2, the microturbulence velocity does not have exactly the same effect for all the methods. The rest of parameters may play a role too, the abundance determination may compensate for the discrepancies from other parameters when enforcing a certain temperature or gravity that does not match what our analysis would have found with our models, codes and set-up.

To visually compare the precision for all the analysed elements at once between all the codes, I added the normalized differences and dispersion and represented them in Figure 23. The results indicate that the pattern observed for iron abundances can be generalized for the rest of elements.

Regarding the accuracy of all the derived individual chemical abundances with fixed atmospheric parameters, equivalent width methods outperform synthesis for calcium abundances but not for the rest of elements. It is worth remembering that the reference chemical abundances were de-

termined by combining spectroscopic results obtained by different groups using their own techniques (abundances cannot be obtained independently from spectroscopy, contrary to the effective temperature and surface gravity). Thus, depending on how many different methods were used, how many stars and elements each group analysed, how results were combined and how outliers were treated or removed (Adibekyan et al. 2015), the reference values may be biased towards one method or code depending on the element. For instance, when considering calcium abundances derived with Turbospectrum but using only lines in common with the groups ULB and GAU from Jofré et al. 2015 (which used synthesis with Turbospectrum) then the median difference and robust standard deviation go down to -0.03 ± 0.08 and -0.01 ± 0.06 , respectively, from the original -0.09 ± 0.11 dex. Similarly, there are several elements where equivalent width codes strongly underperform. For instance, if I consider cobalt results with MOOG EW and I use the same spectra and absorption lines in common with the groups EPI, POR and UCM from Jofré et al. 2015 (which used equivalent width with MOOG) then the median difference and robust standard deviation go than to 0.00 ± 0.05 and 0.00 ± 0.03 and 0.00 ± 0.02 , respectively, from the original 0.22 ± 0.30 dex.

I also showed in Sect 4.2 that microturbulence velocity does not have exactly the same effect for all the methods, thus imposing the same reference value for affects differently each code. To assess this effect, I used Grid and SPECTRUM (i.e., interpolating from a grid of spectra and synthesizing) with their best line selection and I repeated the analysis by first computing the microturbulence velocity and resolution for each star (which will compensate for errors in the reference macroturbulence velocity and rotation) while fixing the rest of parameters to their reference value, and then calculating the iron abundance using the reference parameters plus the microturbulence and resolution found. I obtained 0.00 ± 0.03 and -0.02 ± 0.02 dex for Grid and SPECTRUM respectively, showing lower dispersions than the values -0.05 ± 0.10 and -0.06 ± 0.12 dex obtained with all the parameters fixed.

Finally, when considering derived abundances instead of line-by-line differential ones (i.e., derived abundance for a particular absorption line and target star minus the derived abundance for the same absorption line in the reference star, here the Sun), the accuracy of the results and level of agreement between codes significantly worsens. Line-by-line differential analysis helps reducing systematics such as the ones presented in Sect. 4.1, although the more different the target star is from the reference star, the less effective this strategy is.

4.3.2 Limited Gaia Benchmark Stars dataset

Equivalently to Sect. 4.2.2, to explore a more limited regions of the parameter space that the Gaia Benchmark Stars cover, I selected the individual chemical abundances for the stars with reference effective temperature greater than 4500 K and metallicity higher than -1.0 dex. Then I added the normalized median difference and robust standard dispersion between codes for all the analysed elements as shown in Figure 25. Filtering out stars that are less convenient for the equivalent width method does not erase the systematic

differences already observed in Figure 23 and described in Sect. 4.3.1.

When comparing the results to the reference values as shown in Figure 26, the median differences and robust standard deviations improve for all the codes compared to Figure 24 but more significantly for the equivalent width methods, where also MOOG EW obtains better results in contrast to WIDTH9.

4.4 The non-observed dataset experiment

The analysis of a dataset of 672 normalized synthetic spectra (112 spectra synthesized with the five codes included in this analysis plus 112 interpolated with the pre-computed grid) described in Sect. 3.7 represents a major computational effort with hundreds of CPU hours. Apart from the determination of atmospheric parameters, it has led to the determination of more than two million abundances from more than 60 000 absorption lines analysed with each method and code.

The outcome of this experiment, summarized in Figure 27, reproduces very closely the same main results obtained using the observed dataset. Hence, this ensures that the conclusions from this work are affected by observational biases such as instrument effects, night conditions, raw data processing, or the inability for models to perfectly reproduce physical processes.

4.5 The one variable at a time experiment

The zero point of this experiment (described in Sect. 3.8) is set by the atmospheric parameters of the Sun, the MARCS model atmosphere, the GES atomic line list, the code MOOG for the equivalent width approach and SPECTRUM for synthesis. In all the figures referenced in this section, the zero point is found in the intersection of the horizontal axis and the thick light gray vertical line. The x axis correspond to the independent variable being changed (e.g., effective temperature, electron density) and the y axis is the outcome being evaluated which is very simply computed as:

$$f(x) = \text{median}(v - v_{\text{ref}}) \quad (1)$$

where v is the abundance for equivalent width codes or the depth for synthesis codes, and v_{ref} is the abundance or depth of reference. The dispersion is computed using the absolute median deviation.

4.5.1 Atmospheric parameters

As shown in Figure 28, the equivalent width codes show a systematic discrepancy for lower surface gravities, and it is particularly puzzling the different pattern shown for metallicities between -2.0 and 0.0 dex. The effect of the microturbulence velocity shows a small but increasing systematic when going towards higher values (i.e., it is not just a constant offset between codes). Alpha enhancement does not have an impact on MOOG results, this is most probably because MOOG does not re-compute the electron density but it directly uses the values from the model atmosphere (i.e., changing the alpha parameter does not have an effect

unless a full new model atmosphere is computed with the changed alpha parameter). WIDTH9 leads to more stable results despite significantly reducing the number of layers in the model atmosphere, while MOOG median abundances shows an offset of 0.10 dex when only 12 layers are used instead of the original 56.

Regarding synthesis (see Figures 29 and 30), lower effective temperatures lead to increasing discrepancies in the continuum and absorption line core depths. In the coolest end (2800 K), Turbospectrum and SME are relatively close with the deepest continuum among all the codes, MOOG is on the other end of the range with a continuum depth similar to the Sun. In terms of surface gravity, all the codes compute a continuum depth that is generally in higher agreement for giant stars, while line core depths show the opposite pattern with the exception of MOOG, which is systematically deeper than the rest of codes (the contrary is true for line depths). Changes in metallicity show a high level of agreement for absorption line depths although small discrepancies in continuum depth are present for solar values. Interestingly, variations in alpha abundances lead to very different continuum depth patterns among the codes. The highest agreement is found for absorption line depths with solar alpha abundances, while MOOG and Turbospectrum deviate from the rest for negative values. Microturbulence effects are only evident on the continuum depths, where all the codes keep a extremely small constant difference for all tested values. Finally, when the number of layers in the model atmosphere is reduced, SME is the code that deviates the most from the reference point.

4.5.2 Model atmosphere

From the model atmosphere, equivalent width codes are only affected by changes in column mass, temperature, and gas pressure, plus electron density in the case of MOOG as shown in Figure 31. The highest disagreements happen with variation of temperature values, followed by reductions in gas pressure.

Regarding the results from synthesis codes shown in Figures 32 and 33, no effects are observed when changing the Rosseland mean absorption coefficient, radiation pressure, and microturbulence velocities, plus electron density except in the case of MOOG. Turbospectrum is the only code that uses optical depth instead of column mass and electron pressure instead of gas pressure. In general terms all the codes show differences that remain constant with the exception of variation of temperature and gas pressure.

4.5.3 Atomic line list

All the equivalent width codes (see Figure 34) present very similar results when varying the oscillator strength, but discrepancies appear for the atomic broadening parameters. MOOG does not implement the Stark damping parameter, hence no effect is expected when changing this value. Nevertheless, MOOG also does not show any change when varying the radiative damping parameter. Regarding the van der Waals damping parameter, MOOG and WIDTH9 show an almost constant systematic.

With respect to synthesis codes (see Figure 35 Figure 36), the effects of varying oscillator strength parameters

shows small changing continuum differences between all the codes. MOOG and Turbospectrum do not implement broadening using the Stark damping parameter, thus no effect is observed when it is modified. MOOG does not any effect when varying the radiative damping parameter either. The rest of codes show very small variations in line depths and changes are more noticeable in continuum depth, where different patterns emerge. This reveals clear differences in the implementation of line broadening effects for each code.

5 DISCUSSION

From the 2 496 absorption lines studied in the optical range (480 - 680 nm) of the solar spectrum, only an average of ~ 300 abundances are within the ± 0.10 dex range when using the equivalent width method, and within ± 0.05 when using the synthetic spectral fitting technique. This represents less than 15% of the total number of analysed absorption lines, despite that the Sun is the star of reference that we know the most and the same observed data, normalization process, model atmosphere, solar abundances and atomic data were used by all the codes. When considering a larger margin of ± 0.25 dex, the percentage increases to 50%, 65% and 75% for equivalent width methods, synthesis and interpolation from pre-computed grid of spectra (i.e., Grid), respectively. The equivalent width method suffers from blends, skewing the abundance distribution towards greater abundances (i.e., overestimating abundances from blended lines) and, consequently, presenting a lower number of lines for narrower margins. Grid is the strategy with which a higher number of lines are close to the reference abundance, the reasons are not obvious and it could be a combination of causes such as: 1) model atmosphere are computed with a certain chemical composition (typically directly related to the solar abundances), Grid scales the metallicity and does not alter the individual chemical pattern, thus its coherence with the model atmosphere is maximal contrary to the synthesis codes. 2) For blended absorption lines, synthesis has more margin to derive higher or lower abundances for a particular element, while Grid is more constraint given that all the abundances are being increased/decreased at the same time via the metallicity parameter. As shown in Sect. 4.1, line-by-line comparisons between all the codes show systematics for certain elements and disagreements that depend on the reduced equivalent width of each line (except for synthesis).

The number of good lines in common between equivalent width codes is high, while the average percentage of matching for synthesis codes is around 85%. As explained in Sect. 3.3 and 3.4, using the same model atmosphere and atomic line list does not imply that the synthetic spectrum is going to be computed using the same data since each code may use different values (also shown in Sect. 4.5), there are differences in the implementation of the line broadening parameters (see Sect. 4.5.3), and in the case of synthesis the effect of these differences increases since blends are also taken into account (e.g., near-by lines can influence negatively the results if the atomic data is inaccurate). In addition, it is remarkable how much the average percentage of matching lines decreases when comparing results between an equivalent width code and synthesis one ($\sim 50\%$). The cause can

again related to the intrinsic difference already explained between each approach.

For the different setups evaluated in this work, the codes that lead to more similar results are SME, SYNTHE and SPECTRUM as shown in Figures 10 and 23, although the first one performs worse when using the wings of H- α / β and/or Mg triplet as described in Sect. 4.2. For studies where only the wings of hydrogen lines are used to determine effective temperature, SPECTRUM and SYNTHE produce the results with the smallest systematics and, for all the codes, it is preferable to use H- α over H- β since the latter is not well reproduced as well. In general terms, the most accurate results are obtained with SPECTRUM closely followed by SYNTHE as seen in Figure 13, but the former is faster in terms of computation time. Furthermore, it is worth remembering that all the radiative transfer codes considered in this work use 1D models and assume LTE, overviews of the present and future prospects of 3D-non-LTE models can be found Barklem (2016); Nissen & Gustafsson (2018); Jofré et al. (2018).

Interpolating from a grid of pre-computed synthetic spectra (i.e., Grid) also provides a remarkable good accuracy, despite of being slightly behind SPECTRUM and SYNTHE, it is worth considering given that for a single spectrum it can take an average of 30 minutes to derive atmospheric parameters with synthesis and only 5 minutes with interpolation. Grid requires to have an existing pre-computed grid, which is a computational work that only has to be done once and a grid of $\sim 30\,000$ spectra covering from 480 to 680 nm can be completed in less than a day in a modern machine with 32 CPUs.

When comparing all the codes in a even more controlled experiment (see Sect. 4.4 and 4.5), differences in abundance determinations (equivalent width methods) or synthetic flux computation emerge when any of the input parameters (atmospheric parameters, model atmosphere or atomic data) are varied. This is due to the implementation differences such as continuum calculations and line broadening effects, and it shows how varying discrepancies appear when using the same method (i.e., equivalent width or synthetic spectral fitting) but different codes.

Apart from individual differences between codes, we can also notice that there are some clear systematic between equivalent width methods and the synthetic spectral fitting technique. Limiting the analysed dataset by discarding the cooler and metal poorer stars, which are very challenging type of stars for the equivalent width method, does not fully erase the systematics as shown in Figures 10 and 20. MOOG EW and WIDTH9 lead to a extremely similar results when they use the common line selection but they deviate when using their own line selection. It is particularly interesting that depending if I consider the full or the limited dataset of Gaia Benchmark Stars, it is WIDTH9 or MOOG EW which gets more similar to results from synthesis codes. This shows that the systematics between codes and methods are not independent from the stellar types and this discourages blindly combining results from multiple methods and/or codes.

In general terms, the equivalent width method can only compete with the synthetic spectral fitting technique when the spectral range is limited and the cooler and metal poorer stars (higher number of blends) are not considered, where MOOG EW leads to better results compared to WIDTH9.

The analysis of one spectrum using equivalent widths can take less than a minute and this makes a strong argument for this approach if the target stars are expected to be in the optimal range of parameters.

It is worth mentioning that the high level of precision between codes shown in this work is higher than the level of agreement that one could find between studies from different authors. The tests presented here used a line selection that was executed in a very homogeneous way for all the codes, it can be expected that heterogeneous line selections lead to higher differences between codes. Moreover, the strictly line-by-line differential analysis for the determination of individual chemical elements had a significant effect increasing the precision among codes and methods. This work also shows how the selection of absorption lines and other spectral regions play a very relevant role in terms of accuracy, and this selection should be done using the same pipeline and criteria that is going to be used for the target spectra. Re-using line selection done by other authors using different model atmosphere, atomic data, radiative transfer codes and normalization processes is not going to guarantee the best results. This results also question blindly using the full spectrum to derive atmospheric parameters, given that with our models we are not able to completely reproduce even the Sun, the star that we know the most.

The dependency of the microturbulence velocity with the spectroscopic method seen in this work clearly suggests that re-using microturbulence results from different methods should not be a recommended practice. In the case of synthesis, the same recommendation could be extended to the microturbulence velocity for which different recipes exist (e.g., Gaussian and radial-tangential broadening) and it tends to be degenerated together with the projected rotational velocities and the resolution. Moreover, it is sometimes a common practise to fix some of the atmospheric parameters to values obtained by other independent means (occasionally more accurate) but, for instance, forcing the model to use a certain effective temperature can lead to biases in the rest of free parameters as described in Sect. 4.3. There are advantages from fixing parameters to values derived by more accurate methods, but the effects of that should be carefully assessed and controlled.

Given the results presented in this work, it seems reasonable to consider a given selection of model atmosphere, solar abundances, atomic data, radiative transfer code, normalization procedure, general data treatment and spectral wavelength ranges as a ruler in centimetres (for instance) with a precision of 0.1 cm, while a different selection would equal to a ruler in inches with a precision of 0.1 inches (i.e., 0.254 cm). If we want to compare people's height, it looks pretty clear we would not choose to measure each of them using rulers in different units and with different precisions, homogeneity is relevant unless we know how to transform one unit into another very accurately and the precision of each measurement is comparable. We would not also get much benefit from blindly combining measurements for each person with several different rulers of different units, especially if some of these rulers work worse for a particular type of person (e.g., depending on their body structure), who we measure, what/how we measure and how we combine the results may introduce biases that are not easy to account

for. It is generally preferable to have a controlled and homogeneous measurement process.

The combination of results from different sources would be valuable if it is shown that one method is particularly good for a type of star for which the other methods are less reliable (e.g., as claimed in [Smiljanic et al. 2014](#)). Then the difficult task of combining measurements obtained from different rulers may make sense although the process should correctly weight the strengths of each approach, each method should be assessed using benchmark objects, the strategy should be described in detail and the original individual values (spectrum per spectrum and line by line if it applies) should also be shared. For instance, the current work does not provide any reason to support mixing results from the equivalent width method and the synthetic spectral fitting technique, since, apart from the identified systematics, the former is less reliable for stars with many blends while the latter leads to more robust results for a wider range of parameters. Thus, combining results would not lead to better overall outcome but it will introduce biases and complicate comparisons.

6 CONCLUSIONS

In this work, I expanded iSpec capabilities to derive atmospheric parameters and abundances using several new radiative transfer codes. The user can choose between MOOG and WIDTH9 for equivalent width methods, and between SPECTRUM, Turbospectrum, SME, MOOG and SYNTH for the synthetic spectral fitting technique. In addition, I included the possibility to interpolate from a grid of pre-computed/observed spectra (i.e., Grid), which reduces the analysis time for the determination of atmospheric parameters of a single spectrum down to five minutes or less in a modern computer.

By designing a completely automatic spectroscopic pipeline and analysing the Gaia Benchmark Stars, I executed a complete experiment that explores the key pitfalls of modern spectroscopy by comparing the spectroscopic results (atmospheric parameters and individual chemical abundances) when using several radiative transfer codes and different spectroscopic techniques with multiple setups.

The results showed that the synthetic spectral technique has a higher accuracy when considering the full range of atmospheric parameters that the Gaia Benchmark Stars cover, while the equivalent width can be competitive only when the dataset is limited by discarding cooler and metal poorer stars. When the right set-up is selected, interpolating from a grid of pre-computed spectra has an accuracy almost comparable to the results obtained when using synthesis with interpolated model atmosphere. To reach the best results, a proper line selection should be executed using the same model atmosphere, atomic data, radiative transfer code and normalization process that will be applied to the target spectra. In the case of synthesis, including the wings of H- α / β and Mg triplet can help increase the accuracy when using Grid, SPECTRUM and SYNTH codes.

Despite using a homogeneous process to select the best common absorption lines, there are clear systematics between the equivalent width method and the synthetic spectral fitting technique. In addition, for the latter, there are

also differences when interpolating from a pre-computed grid of spectra or synthesizing with an interpolated atmospheric model. This demonstrated that blindly combining atmospheric parameters and chemical abundances measured using heterogeneous setups and methods is not a recommended procedure, especially when high-precision is key for the scientific goals of the study.

This study undercover code-to-code differences that can affect the scientific interpretation of spectroscopic analysis, this suggests that it would be a good practise to assess if the conclusions still hold when deriving the same atmospheric parameters and/or abundances with different codes.

There are plenty of models and tools freely accessible today to analyse the growing number of high-quality spectra available in the public archives or to execute our own observations and studies. This easy-access scenario represents an unprecedented opportunity in the history of stellar spectroscopy to expand, grow and discover the wonders of the stars but simultaneously, it carries the responsibility of carefully considering the modern spectroscopy caveats exposed here.

ACKNOWLEDGEMENTS

This research has made use of NASA’s Astrophysics Data System. This work would not have been possible without the invaluable contribution from all the authors that developed the considered radiative transfer codes: Richard O. Gray, Robert L. Kurucz, Luca Sbordone, Nikolai Piskunov, Jeff A. Valenti, Bertrand Plez, Chris Sneden plus any other major contributor that I may have forgotten. In the same sense, Bengt Gustafsson and contributors should be acknowledge for their major contribution to stellar astrophysics with their MARCS model atmosphere. Additionally, I am very grateful to Thomas Nordlander, Ulrike Heiter, Paula Jofré, Thomas Masseron, Laia Casamiquela, Hugo M. Tabernero, Andrew R. Casey, Jorge Meléndez, and Ivan Ramírez for their help integrating and testing all these radiative transfer codes in iSpec. I thank the anonymous referee who has significantly improved the quality of this work with great ideas and suggestions.

REFERENCES

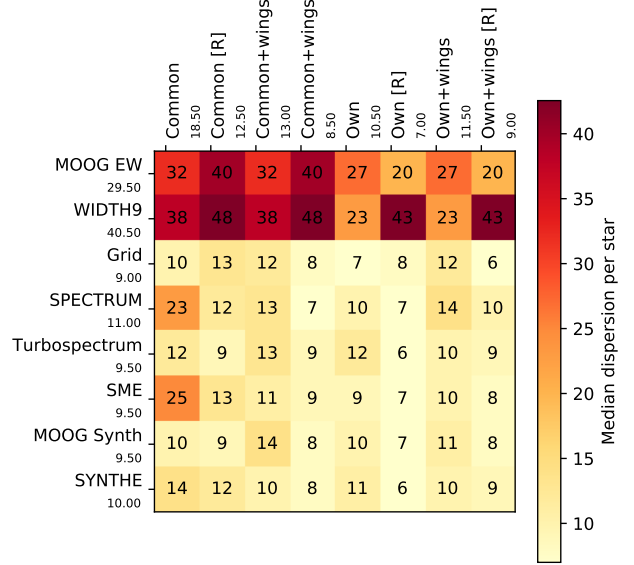
- Adibekyan V., et al., 2015, *A&A*, **583**, A94
- Ali A. W., Griem H. R., 1965, *Physical Review*, **140**, 1044
- Ali A. W., Griem H. R., 1966, *Physical Review*, **144**, 366
- Allende Prieto C., Beers T. C., Wilhelm R., Newberg H. J., Rockosi C. M., Yanny B., Lee Y. S., 2006, *ApJ*, **636**, 804
- Alvarez R., Plez B., 1998, *A&A*, **330**, 1109
- Anstee S. D., O’Mara B. J., 1991, *MNRAS*, **253**, 549
- Anstee S. D., O’Mara B. J., 1995, *MNRAS*, **276**, 859
- Astropy Collaboration et al., 2013, *A&A*, **558**, A33
- Barber C. B., Dobkin D. P., Huhdanpaa H., 1996, *ACM Trans. Math. Softw.*, **22**, 469
- Barklem P. S., 2016, *Astronomy and Astrophysics Review*, **24**, 9
- Barklem P. S., Piskunov N., O’Mara B. J., 2000, *A&A*, **363**, 1091
- Barklem P. S., Stempels H. C., Allende Prieto C., Kochukhov O. P., Piskunov N., O’Mara B. J., 2002, *A&A*, **385**, 951
- Blanco-Cuaresma S., 2017, in EWASS Special Session 4 (2017): Star-planet interactions (EWASS-SS4-2017. , doi:10.5281/zenodo.1056914
- Blanco-Cuaresma S., Fraix-Burnet D., 2018, preprint, [p. arXiv:1807.03787](https://arxiv.org/abs/1807.03787) ([arXiv:1807.03787](https://arxiv.org/abs/1807.03787))
- Blanco-Cuaresma S., Soubiran C., 2016, in SF2A-2016: Proceedings of the Annual meeting of the French Society of Astronomy and Astrophysics. pp 333–336
- Blanco-Cuaresma S., Soubiran C., Jofré P., Heiter U., 2014a, *A&A*, **566**, A98
- Blanco-Cuaresma S., Soubiran C., Heiter U., Jofré P., 2014b, *A&A*, **569**, A111
- Blanco-Cuaresma S., et al., 2015, *A&A*, **577**, A47
- Blanco-Cuaresma S., et al., 2017, in Highlights on Spanish Astrophysics IX. pp 334–337
- Brahm R., Jordán A., Hartman J., Bakos G., 2017, *MNRAS*, **467**, 971
- Buitinck L., et al., 2013, in ECML PKDD Workshop: Languages for Data Mining and Machine Learning. pp 108–122
- Casamiquela L., et al., 2016, *MNRAS*, **458**, 3150
- Casamiquela L., et al., 2017, *MNRAS*, **470**, 4363
- Casey A. R., 2016, *ApJS*, **223**, 8
- Cayrel R., van’t Veer-Menneret C., Allard N. F., Stehlé C., 2011, *A&A*, **531**, A83
- Cowley C. R., Castelli F., 2002, *A&A*, **387**, 595
- Czekala I., Andrews S. M., Mandel K. S., Hogg D. W., Green G. M., 2015, *ApJ*, **812**, 128
- Eisenstein D. J., et al., 2011, *AJ*, **142**, 72
- Gilmore G., et al., 2012, *The Messenger*, **147**, 25
- Giribaldi R. E., Ubaldo-Melo M. L., Porto de Mello G. F., Pasquini L., Ludwig H.-G., Ulmer-Moll S., Lorenzo-Oliveira D., 2018, arXiv e-prints, [p. arXiv:1811.12274](https://arxiv.org/abs/1811.12274)
- Gray D. F., 2008, *The Observation and Analysis of Stellar Photospheres*
- Gray R. O., Corbally C. J., 1994, *AJ*, **107**, 742
- Grevesse N., Asplund M., Sauval A. J., 2007, *Space Sci. Rev.*, **130**, 105
- Gustafsson B., Edvardsson B., Eriksson K., Jørgensen U. G., Nordlund Å., Plez B., 2008, *A&A*, **486**, 951
- Hawkins K., et al., 2016, *A&A*, **592**, A70
- Heiter U., Eriksson K., 2006, *A&A*, **452**, 1039
- Heiter U., et al., 2015a, *Phys. Scr.*, **90**, 054010
- Heiter U., Jofré P., Gustafsson B., Korn A. J., Soubiran C., Thévenin F., 2015b, *A&A*, **582**, A49
- Hinkel N. R., Timmes F. X., Young P. A., Pagano M. D., Turnbull M. C., 2014, *AJ*, **148**, 54
- Hinkel N. R., et al., 2016, *ApJS*, **226**, 4
- Hinkle K., Wallace L., Valenti J., Harmer D., 2000, *Visible and Near Infrared Atlas of the Arcturus Spectrum 3727-9300 Å*
- Hubeny I., Lanz T., 2011, *Synspec: General Spectrum Synthesis Program* (ascl:1109.022)
- Jofré P., et al., 2014, *A&A*, **564**, A133
- Jofré P., et al., 2015, *A&A*, **582**, A81
- Jofré P., et al., 2017, *A&A*, **601**, A38
- Jofré P., Heiter U., Soubiran C., 2018, arXiv e-prints, [p. arXiv:1811.08041](https://arxiv.org/abs/1811.08041)
- Jones E., Oliphant T., Peterson P., et al., 2001, *SciPy: Open source scientific tools for Python*, <http://www.scipy.org/>
- Koleva M., Prugniel P., Bouchard A., Wu Y., 2009, *A&A*, **501**, 1269
- Kurucz R., 1993, *SYNTHES Spectrum Synthesis Programs and Line Data*. Kurucz CD-ROM No. 18. Cambridge, Mass.: Smithsonian Astrophysical Observatory, 1993., **18**
- Majewski S. R., et al., 2017, *AJ*, **154**, 94
- Mucciarelli A., Pancino E., Lovisi L., Ferraro F. R., Lapenna E., 2013, *ApJ*, **766**, 78
- Ness M., Hogg D. W., Rix H.-W., Ho A. Y. Q., Zasowski G., 2015, *ApJ*, **808**, 16
- Niemczura E., Smalley B., Pych W., 2014, *Determination of Atmospheric Parameters of B-, A-, F- and G-Type Stars*, doi:10.1007/978-3-319-06956-2.

- Nissen P. E., Gustafsson B., 2018, *Astronomy and Astrophysics Review*, **26**, 6
- Pedregosa F., et al., 2011, *Journal of Machine Learning Research*, **12**, 2825
- Plez B., 2012, *Turbospectrum: Code for spectral synthesis*, Astrophysics Source Code Library (ascl:1205.004)
- Randich S., Gilmore G., Gaia-ESO Consortium 2013, *The Messenger*, **154**, 47
- Recio-Blanco A., Bijaoui A., de Laverny P., 2006, *MNRAS*, **370**, 141
- Sbordone L., Bonifacio P., Castelli F., Kurucz R. L., 2004, *Memorie della Societa Astronomica Italiana Supplementi*, **5**, 93
- Smiljanic R., et al., 2014, *A&A*, **570**, A122
- Snedden C., Bean J., Ivans I., Lucatello S., Sobek J., 2012, *MOOG: LTE line analysis and spectrum synthesis*, Astrophysics Source Code Library (ascl:1202.009)
- Tabernero H. M., González Hernández J. I., Montes D., 2013, in Guirado J. C., Lara L. M., Quilis V., Gorgas J., eds, *Highlights of Spanish Astrophysics VII*. pp 673–673
- The Astropy Collaboration et al., 2018, preprint, ([arXiv:1801.02634](https://arxiv.org/abs/1801.02634))
- Tsantaki M., Andreasen D. T., Teixeira G. D. C., Sousa S. G., Santos N. C., Delgado-Mena E., Bruzual G., 2018, *MNRAS*, **473**, 5066
- Valenti J. A., Piskunov N., 1996, *A&AS*, **118**, 595
- Vollmann K., Eversberg T., 2006, *Astronomische Nachrichten*, **327**, 862

APPENDIX A: MODEL ATMOSPHERE AND ATOMIC DATA

This paper has been typeset from a \LaTeX file prepared by the author.

:: Δteff (dispersion) per star



:: $\Delta\log g$ (dispersion) per star

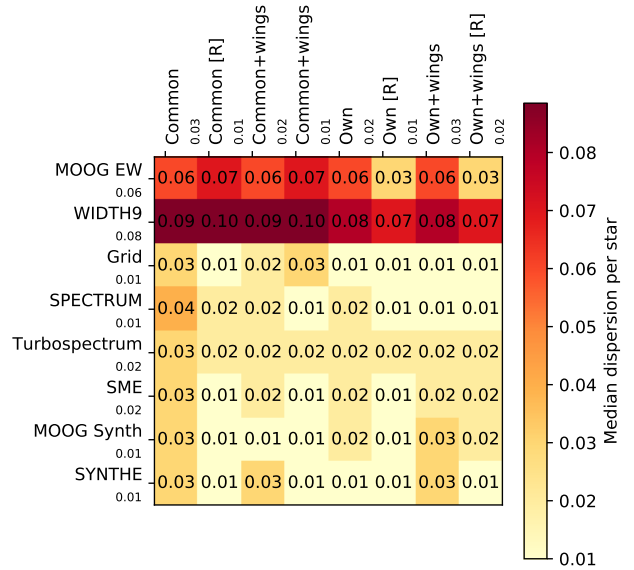


Figure 12. Median robust standard deviation of the effective temperature and surface gravity per star (when multiple spectra were available) when analysing the Gaia Benchmark Stars and using different radiative transfer codes with several setups: using lines in common within equivalent width and synthesis methods, using the best lines for each code (i.e. their own lines, not necessarily good for other codes), using the wings of H- α / β and Mg triplet, repeating the normalization (labelled with [R]) but using a synthetic spectrum that matches the atmospheric parameters found in the first iteration.

	SPECTRUM	Turbospectrum	SME	MOOG	WIDTH9/SYNTH
Column mass above each point [g cm^{-2}]	✓		✓	✓	✓
Temperature [K]	✓	✓	✓	✓	✓
Gas pressure [dyn cm^{-2}]	✓	✓	✓	✓	✓
Electron density [cm^{-3}]	✓		✓	✓	✓
Rosseland mean absorption coefficient [$\text{cm}^2 \text{g}^{-1}$]	✓				✓
Radiation pressure [dyn cm^{-2}]	✓				✓
Microturbulence velocity [m s^{-1}]	✓				✓
Optical depth [$\log \tau$ at 5000 \AA]		✓			
Depth [cm]		✓	✓		
Electron pressure [$\text{cm}^2 \text{g}^{-1}$]		✓			
Turbulence pressure [dyn cm^{-2}]		✓			

Table A1. Model atmosphere fields required as input values for each radiative transfer code. This list respects the expected input order as required by the used version of iSpec.

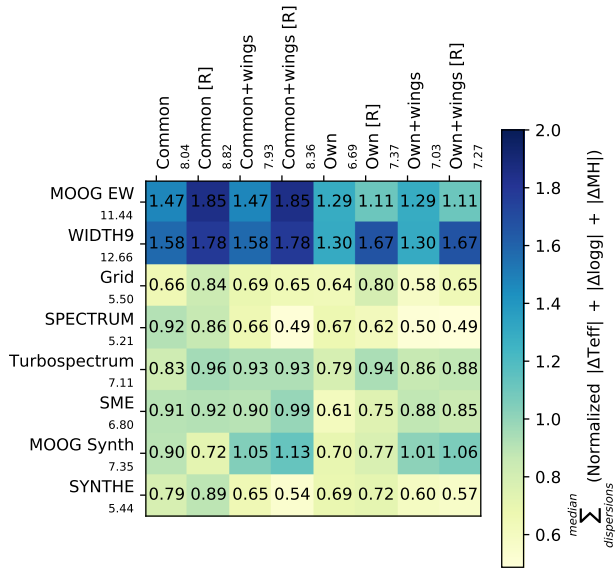


Figure 13. Sum of the normalized absolute median differences with respect to the reference values, normalized robust standard deviation and normalized median robust standard deviation for effective temperature, surface gravity and metallicity when analysing the Gaia Benchmark Stars. Lower numbers indicate results closer to reference values and lower dispersion (higher accuracy).

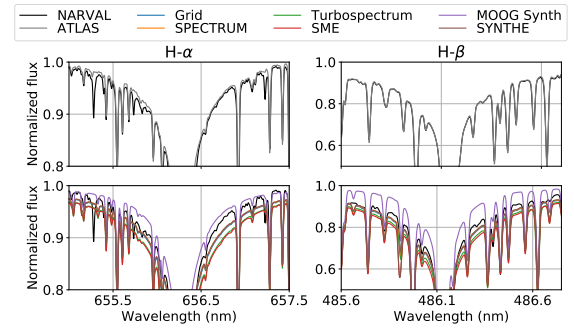


Figure 14. Hydrogen line regions from a NARVAL observed solar spectrum and the solar ATLAS (top), plus the same NARVAL observed solar spectrum and the corresponding synthetic spectra generated with each code (bottom).

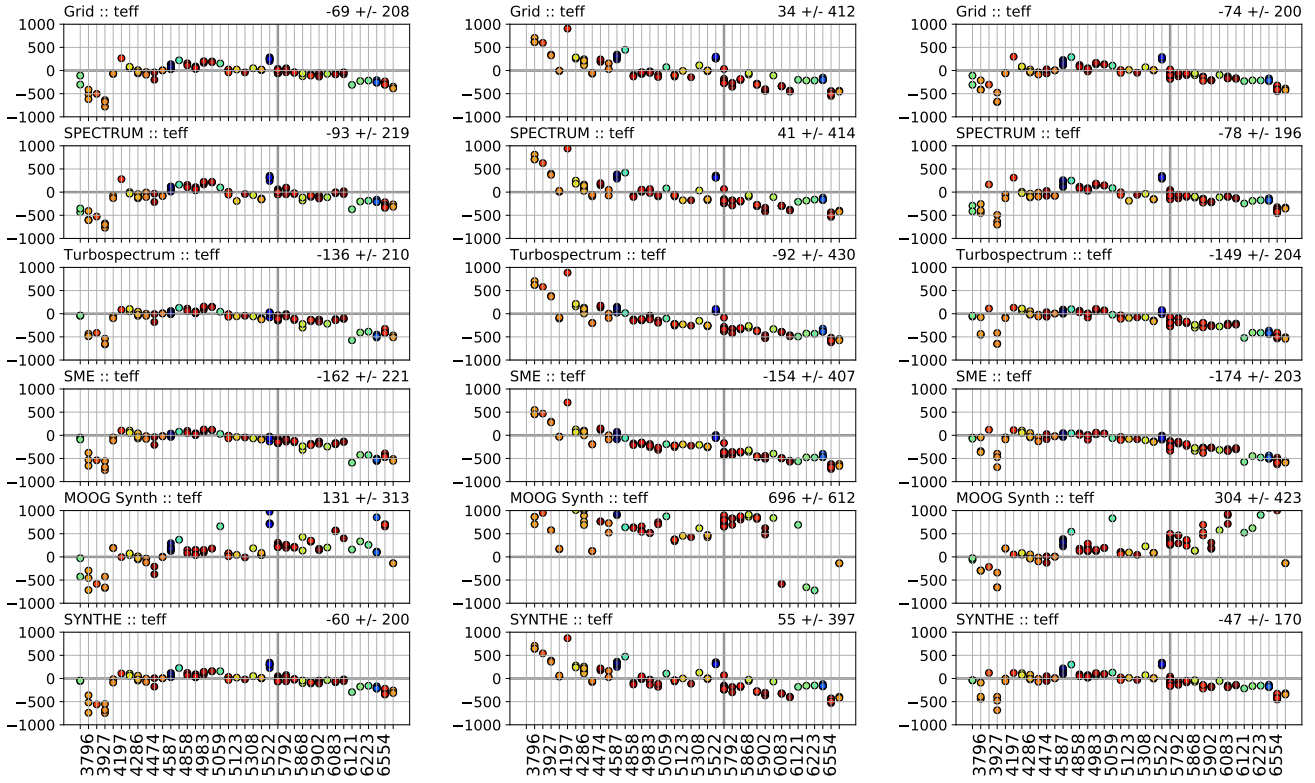


Figure 15. Difference between the derived effective temperature and its reference value for each spectra analyzed with the synthetic spectral fitting codes when using only the wings of H- α (left subplots), H- β (middle subplots) and both of them together (right subplots). The vertical thick gray line denotes the Sun. The color coding represent the metallicity of each star (see right subplots in Figure 16 for color code interpretation). All the subplots are sorted taking into account the reference effective temperature. Median and absolute median deviation are indicated on the upper right of each subplot.

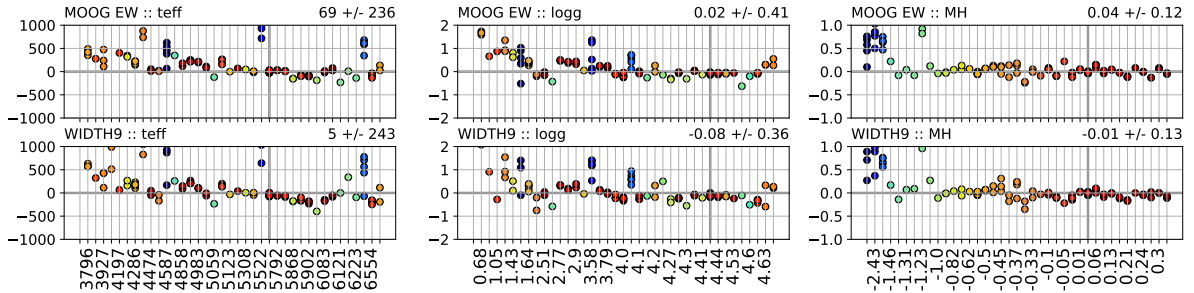


Figure 16. Difference between the derived parameter and its reference value for each spectra analyzed with the equivalent method width when using their best line selection (i.e., own lines). The vertical thick gray line denotes the Sun. The color coding represent the metallicity of each star. All the subplots are sorted taking into account the reference value of the corresponding atmospheric parameter. Median and absolute median deviation are indicated on the upper right of each subplot.

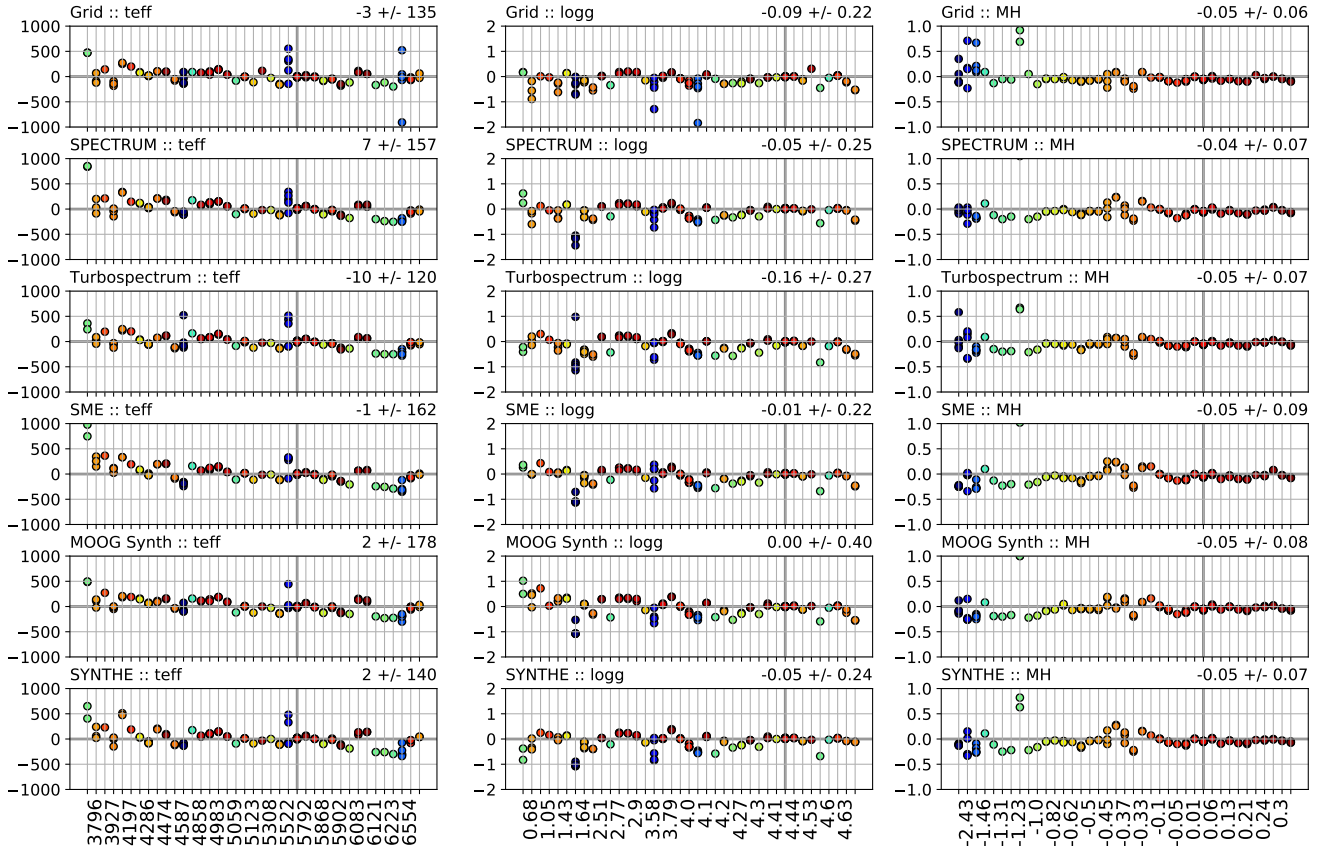


Figure 17. Same as in Figure 16 but for spectra analyzed with the synthetic spectral fitting technique.

	SPECTRUM	Turbospectrum	SME	MOOG	WIDTH9/SYNTH
Element name	✓	✓	✓	✓	
Wavelength [Å]	✓	✓	✓	✓	
Wavelength [nm]					✓
loggf	✓	✓	✓	✓	✓
Lower state [eV]		✓	✓	✓	
Lower state [cm ⁻¹]	✓				✓
Lower j or total angular momentum quantum number					✓
Upper state [eV]					
Upper state [cm ⁻¹]					✓
Upper j or total angular momentum quantum number					✓
Upper g or statistical weight		✓			
Lower Landé g-factor					✓
Upper Landé g-factor					✓
Transition type:	✓				✓
10 to the power of the radiative damping parameter		✓		✓	
Radiative damping parameter	✓		✓		✓
Stark damping parameter	✓		✓		✓
van der Waals damping parameter ($\sigma.\alpha$ format for AO theory)	✓		✓		
van der Waals damping parameter (classic)				✓	✓
Fudge factor (common for the same atomic number and ion) or van der Waals damping parameter (classic or AO theory) if present		✓			
Fudge factor (always set to 1.0)	✓				
Lower orbital type		✓			
Upper orbital type		✓			
Line due to molecular absorption (True/False)	✓	✓	✓	✓	✓
Isotope in spectrum format	✓				✓
Ion (e.g., 0 for neutral lines, 1 for ionized)		✓	✓		
Species code: "atomic number" + "." + "ion state - 1"	✓			✓	
Species code: "atomic number" + "." + "isotope code"		✓			
Species code: "atomic number" + ".0" + "ion state - 1"					✓

Table A2. Atomic line list fields required as input values for each radiative transfer code. Transition type indicates whether the α and σ parameters used in the Anstee and O'Mara broadening theory (Anstee & O'Mara 1991, 1995) are provided (Anstee & O'Mara 1991, 1995, coded as AO type;) or the classic van der Waals broadening should be used (GA type) as described in SPECTRUM documentation. Fudge factors are arbitrary non-physical values used to increase the line broadening to compensate for unknowns. This list respects the expected input order as required by the used version of iSpec.

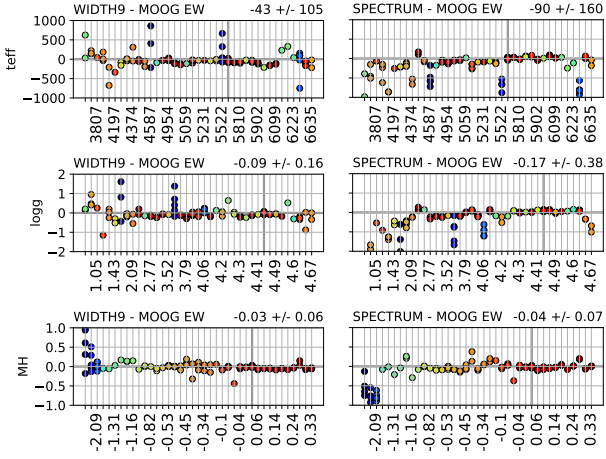


Figure 18. Differences between the two equivalent widths (left subplots), and one code from each method (right subplots) when using their best line selection (i.e., own lines). The vertical thick gray line denotes the Sun. The color coding represent the metallicity of each star. All the subplots are sorted taking into account the reference value of the corresponding atmospheric parameter. Median and absolute median deviation are indicated on the upper right of each subplot.

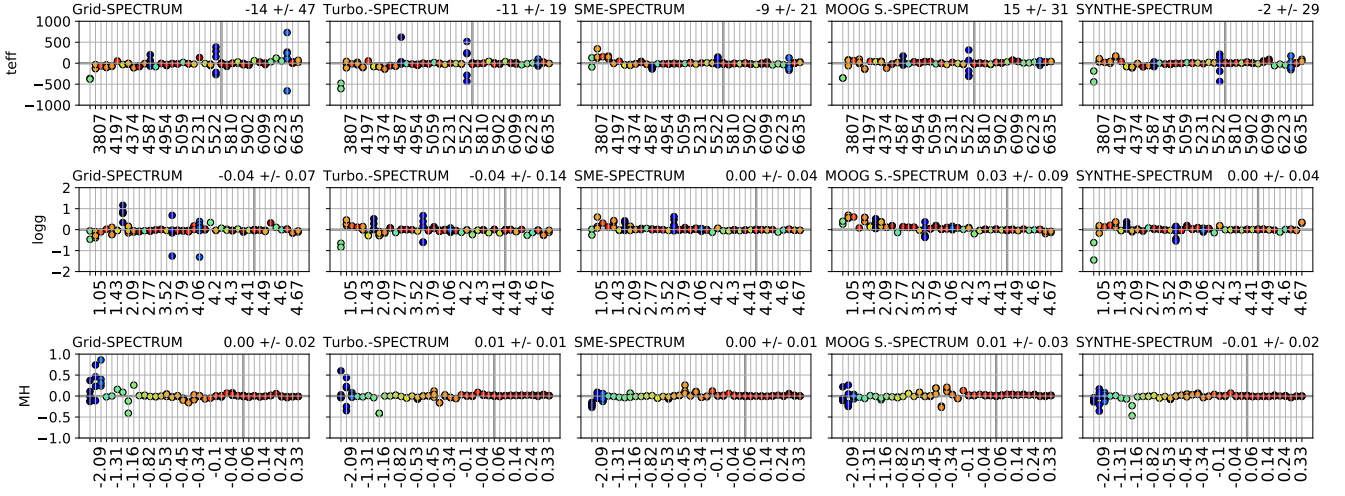


Figure 19. Same as in Figure 18 but only for the synthetic spectral fitting technique.

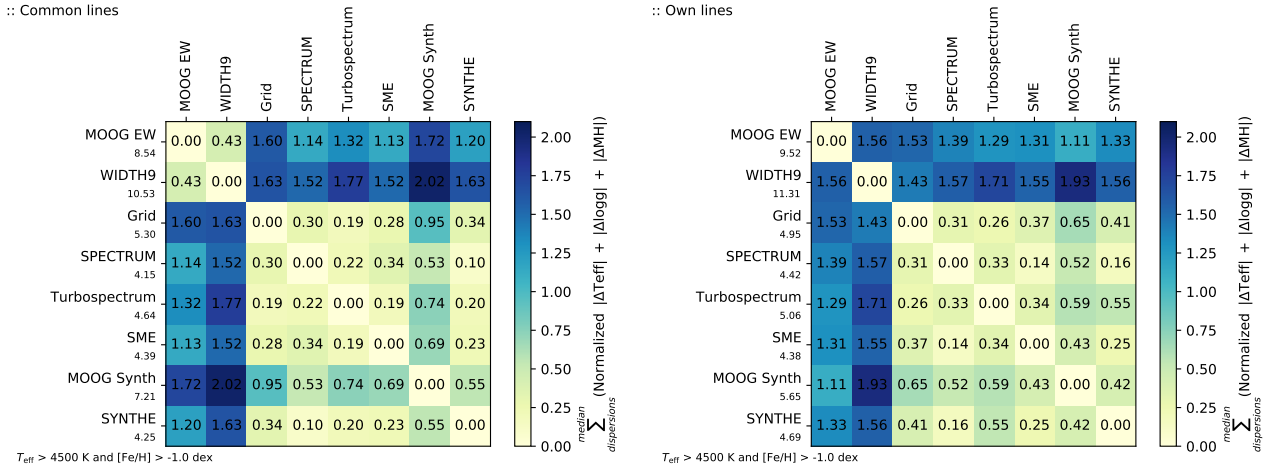


Figure 20. Same as in Figure 10 but considering only Gaia Benchmark Stars with effective temperatures greater than 4500 K and metallicities greater than -1.0 dex.

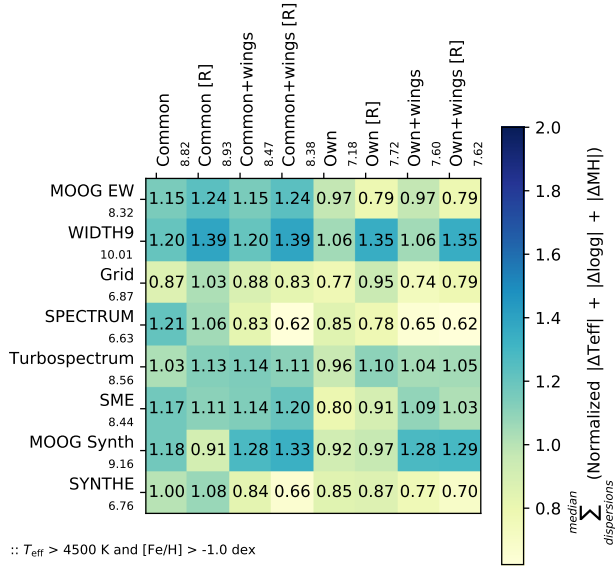


Figure 21. Same as in Figure 13 but considering only Gaia Benchmark Stars with effective temperatures greater than 4500 K and metallicities greater than -1.0 dex.

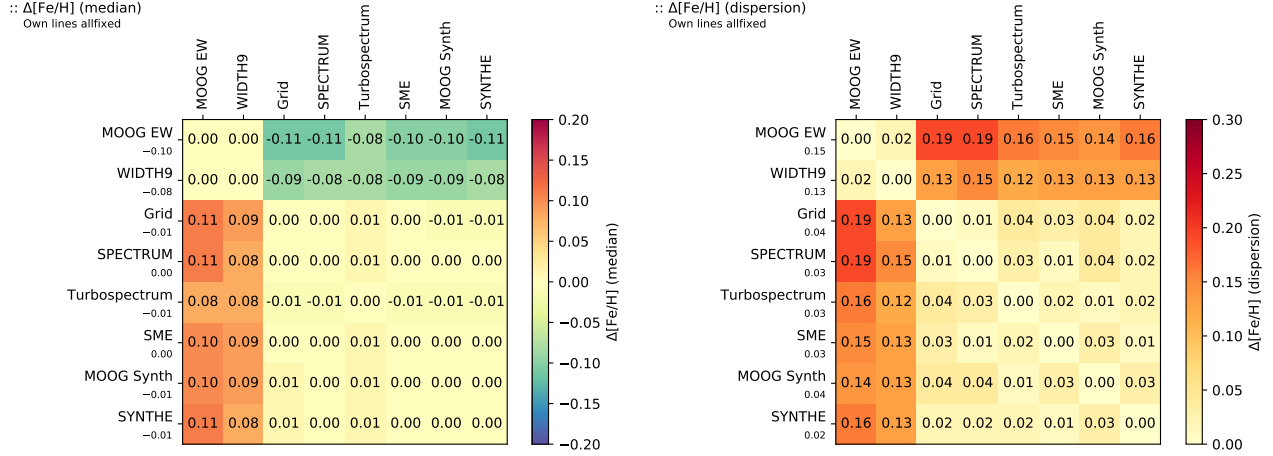


Figure 22. Median and robust standard deviation of the difference in iron abundance between different radiative transfer codes when analysing the Gaia Benchmark Stars and fixing all the atmospheric parameters to the reference ones and using the best line selection for each code.

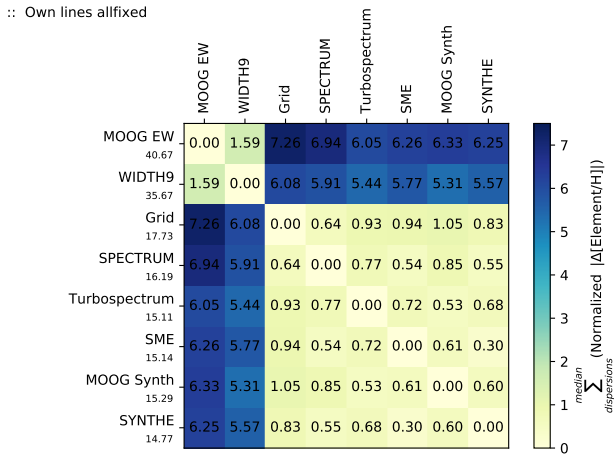


Figure 23. Sum of the normalized absolute median differences and robust standard deviation with respect to other codes for iron, calcium, cobalt, chromium, magnesium, manganese, nickel, silicon, titanium and vanadium abundances when analysing the Gaia Benchmark Stars. Lower numbers indicate the codes lead to more similar results (higher precision).

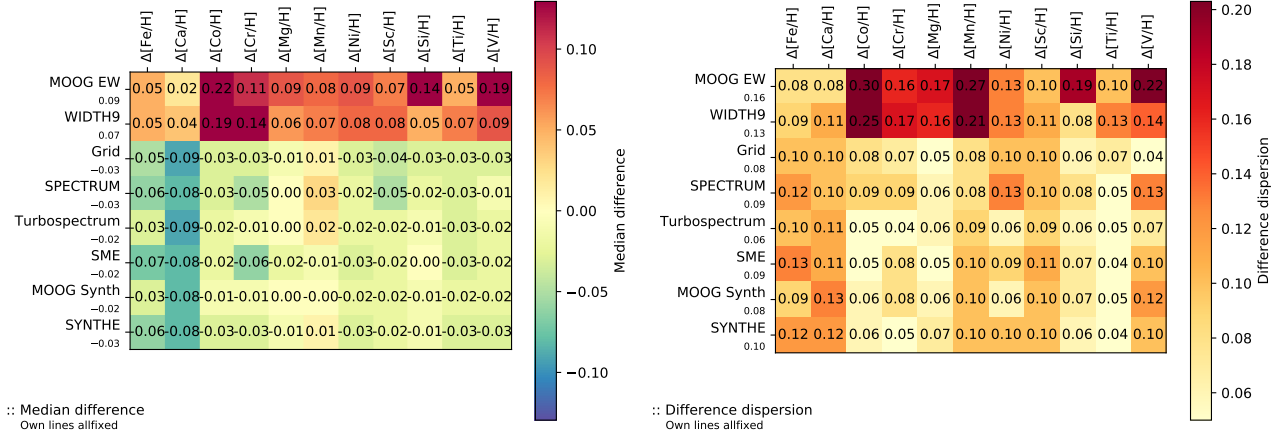


Figure 24. Median and robust standard deviation of the difference in individual abundances between the reference values and different radiative transfer codes when fixing all the atmospheric parameters to the reference ones when analysing the Gaia Benchmark Stars. The best line selection for each code was used. The median dispersion per star is equal or below 0.02 dex for all the cases.

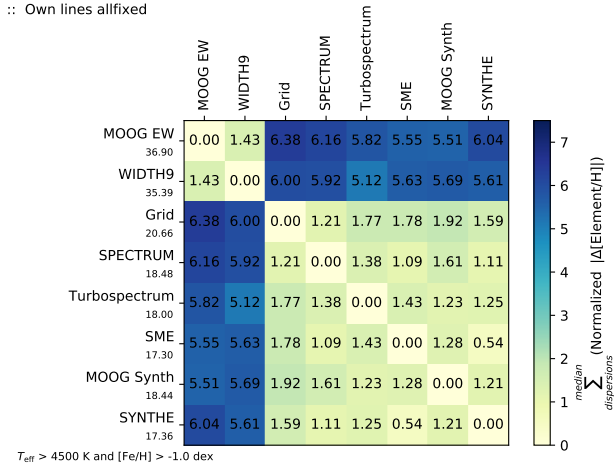


Figure 25. Same as in Figure 23 but considering only Gaia Benchmark Stars with effective temperatures greater than 4500 K and metallicities greater than -1.0 dex.

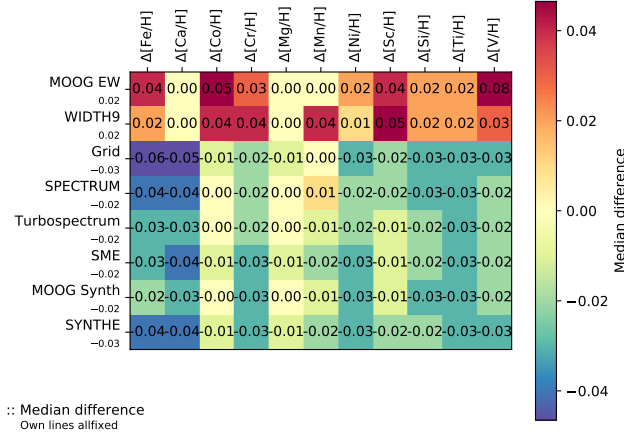
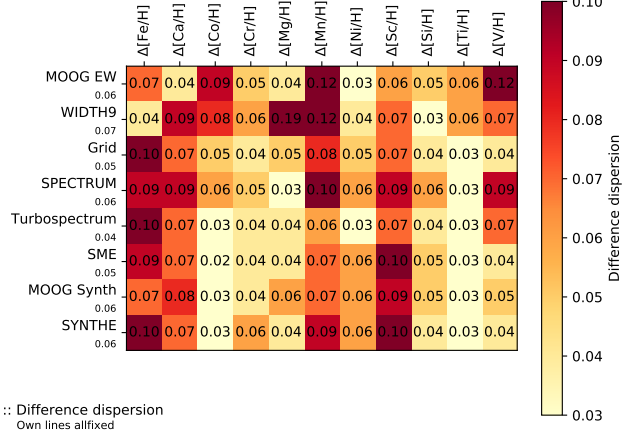
* $T_{\text{eff}} > 4500$ K and $[\text{Fe}/\text{H}] > -1.0$ dex* $T_{\text{eff}} > 4500$ K and $[\text{Fe}/\text{H}] > -1.0$ dex

Figure 26. Same as in Figure 24 but considering only Gaia Benchmark Stars with effective temperatures greater than 4500 K and metallicities greater than -1.0 dex.

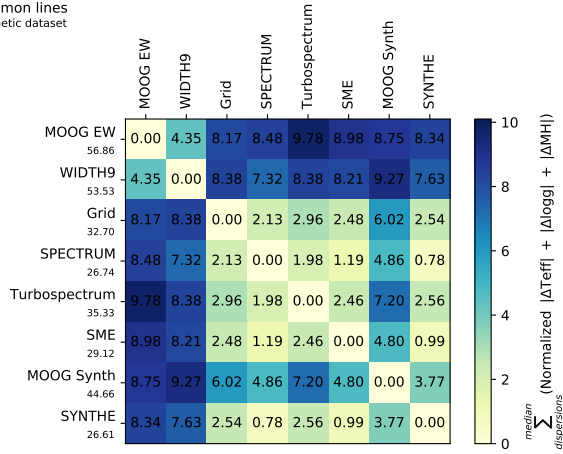
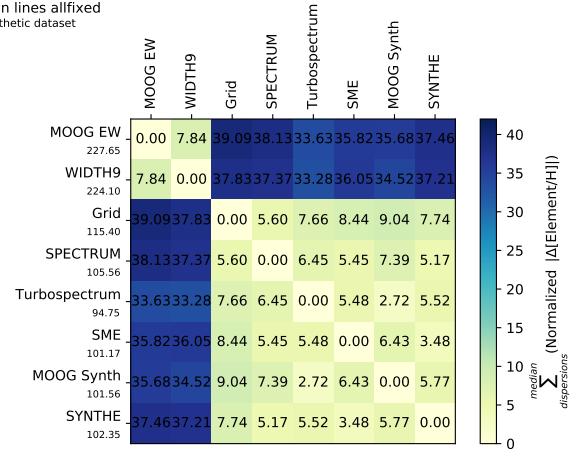
:: Common lines
Synthetic dataset:: Own lines allfixed
Synthetic dataset

Figure 27. Same as in Figures 10 and 23 (left and right plots, respectively) but using the results from the analysis of the synthetic spectra built for the non-observed dataset experiment.

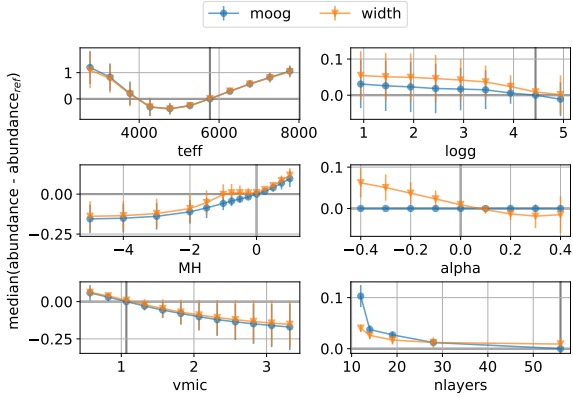


Figure 28. Median and absolute median deviation (error bars) difference in abundance over reference abundance (i.e., MOOG abundances for the Sun, zero point represented by the intersection of the two thick grey lines) when varying different atmospheric parameters and setting the rest to the reference values for the Sun. The lower right plot shows the results when all the atmospheric parameters are set to the solar reference and the number of layers in the atmospheric model are reduced.

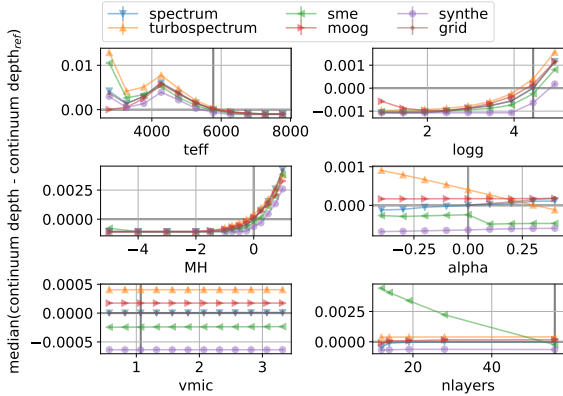


Figure 29. Median difference in continuum depth around 556.45 nm over reference continuum depth (i.e., SPECTRUM continuum depth for the Sun, zero point represented by the intersection of the two thick grey lines) when varying different atmospheric parameters and setting the rest to the reference values for the Sun. The lower right plot shows the results when all the atmospheric parameters are set to the solar reference and the number of layers in the atmospheric model are reduced.

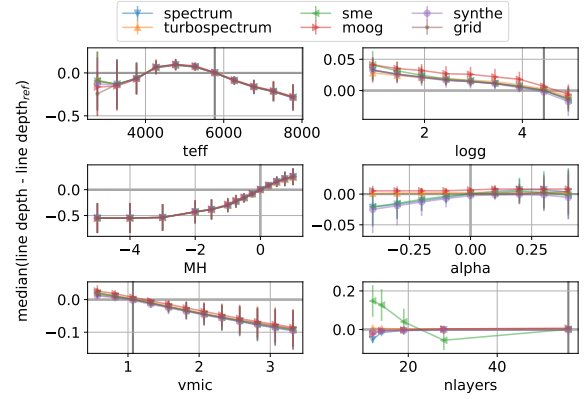


Figure 30. Same as in Figure 29 but considering the depth at the line peaks for the common selection.

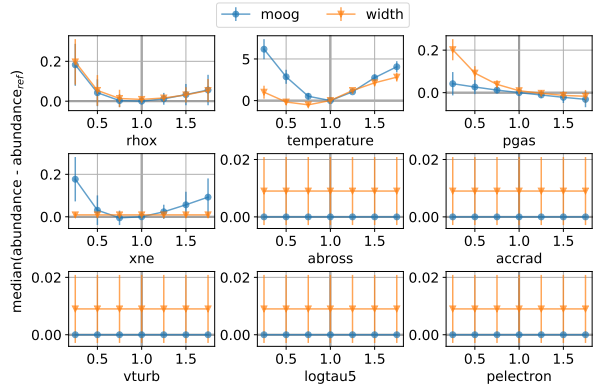


Figure 31. Median and absolute median deviation (error bars) difference in abundance over reference abundance (i.e., MOOG abundances for the Sun, zero point represented by the intersection of the two thick grey lines) when varying different values of the solar model atmosphere.

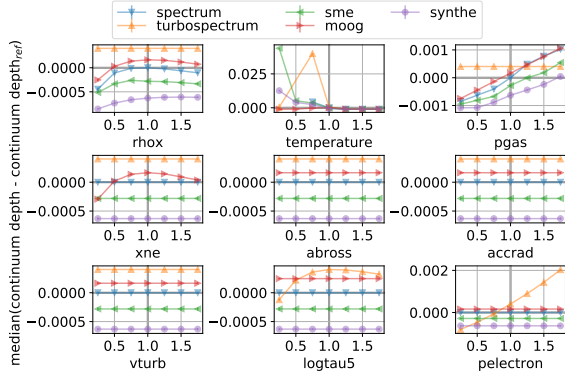


Figure 32. Median and absolute median deviation (error bars) in continuum depth around 556.45 nm over reference continuum depth (i.e., SPECTRUM continuum depth for the Sun, zero point represented by the intersection of the two thick grey lines) when varying different values of the solar model atmosphere.

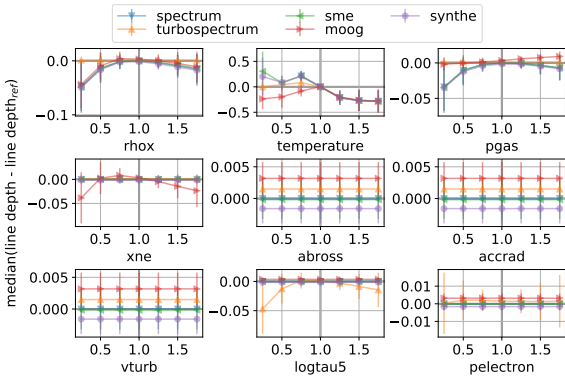


Figure 33. Same as in Figure 32 but considering the depth at the line peaks for the common selection.

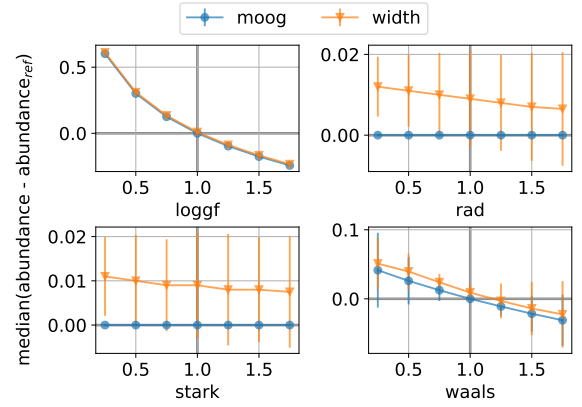


Figure 34. Median and absolute median deviation (error bars) difference in abundance over reference abundance (i.e., MOOG abundances for the Sun, zero point represented by the intersection of the two thick grey lines) when varying different values of the atomic line list.

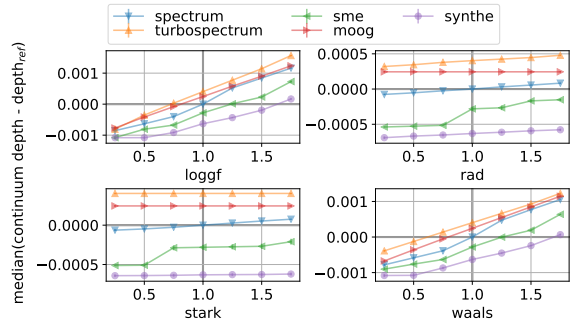


Figure 35. Median and absolute median deviation (error bars) difference in continuum depth around 556.45 nm over reference continuum depth (i.e., SPECTRUM continuum depth for the Sun, zero point represented by the intersection of the two thick grey lines) when varying different values of the atomic line list.

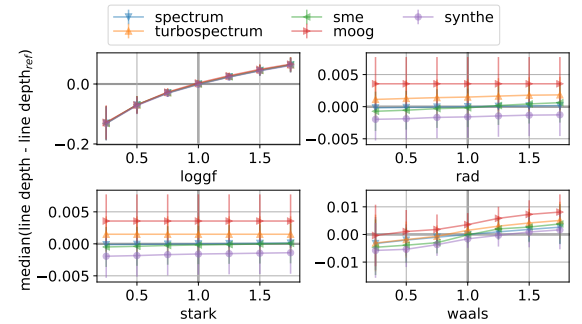


Figure 36. Same as in Figure 35 but considering the depth at the line peaks for the common selection.